



FAKULTÄT FÜR  
INFORMATIK

Otto-von-Guericke University Magdeburg

Faculty of Computer Science

Department of Simulation and Graphics

# Advanced Bone Visualization

## Bachelor-Thesis

in Study

Computer Visualistics

Author: **Hannes Martinke**

Matriclenumber: 199999

Supervisor: **Prof. Dr.-Ing. Bernhard Preim**

Department of Simulation and Graphics

Supervisor: **Dr.-Ing. Michael Suehling**

Siemens Healthcare GmbH

13.03.2017

---

## Declaration of Authorship

I hereby declare that this thesis has been composed by me and is based on my own work, unless stated otherwise. No other person's work has been used without due acknowledgment in this thesis. All references and verbatim extracts have been quoted, and all sources of information have been specifically acknowledged.

Magdeburg, 13.03.2017

.....  
Hannes Martinke

---

## Abstract

This thesis presents a completely new visualization technique for bones with arbitrary elongated structure by CT data. As example the ribs and the vertebrae are used. The diagnosis of ribs by the radiologist is very difficult with current methods (MPR, Rib Unfolding). Therefore he must either slice through the CT slices to navigate, that he can analyze the ribs, or he uses a visualization software with unfolded ribs to inspect them. The problem of this method is that there is only a visualization of the planar cross-section and he need many interaction steps for the diagnosis. The method in this thesis involves two parts. At first, the bone will be segmented and separated in the cortical and spongy layer. The second part is an unwinding of each layer. By doing this the complete surface of the bone is visible in one projection. The radiologist has the ability to recognize rib fractures or metastasis by considering one visualization direct. By marking the suspicious region in the original data he can verify the diagnosis. The created slices can be summarized and combined with a projection method (maximum-intensity-projection, minimum-intensity-projection, average) to display deeper features of the ribs. This supports the different diagnosis types. After that the visualization algorithm was included in the Siemens Healthcare prototype, which served as user interface.

---

## Kurzbeschreibung

Die vorliegende Bachelorarbeit präsentiert eine neuartige Visualisierungsmethode von Knochen beliebiger elongierte Struktur aus CT-Bilddaten, anhand der Rippen und der dazugehörigen Wirbelsäule. Die Diagnose von Rippen ist dem befundenden Radiologen mit bisherigen Methoden (MPR, Rib Unfolding) nur mit hohem Aufwand möglich. Hierzu muss er entweder durch die CT-Schichten hindurch navigieren, so dass die Rippen nacheinander betrachtet werden können, oder mit Hilfe einer geeigneten Visualisierungssoftware die entfalteten Rippen inspizieren, die jedoch nur in entlang von planaren Schnittebenen visualisiert werden und Interaktionsschritte zur Befundung nötig sind. Das hier vorgestellte Verfahren umfasst zwei Teile. Zum einen werden die Knochen segmentiert und jeweils der kortikale Knochen und der spongiöse Teil voneinander getrennt. Im zweiten Teil werden die Layer durch verschiedene Raycasting Methoden abgerollt. Somit ist die gesamte Oberfläche in der Projektion sichtbar und der befundende Radiologe ist somit in der Lage, Rippenbrüche und Metastasen durch Betrachten einer einzelnen Visualisierung sofort zu erkennen und gegebenenfalls an den Original-Schichtdaten durch Markieren einer verdächtigen Region zu verifizieren. Durch das Abrollen der Rippen werden unterschiedliche Befundungen unterstützt und mit einer entsprechenden Projektionsmethode (z.B. Maximum-Intensitäts-Projektions, Minimum-Intensitäts-Projektion, oder Mittelung) können die entstehenden Schichten zu einem Stapel zusammengefasst werden, um tieferliegende Merkmale der Rippen darstellen zu können. Diese Visualisierungsmethode wurde im Anschluss in einem Siemens Healthcare Prototypen eingebaut, welcher als User Interface dient.



---

# Contents

Declaration of Authorship . . . . .	I
Abstract . . . . .	II
Kurzbeschreibung . . . . .	III
<b>1 Introduction</b>	<b>1</b>
1.1 Motivation . . . . .	1
1.2 Thesis Task . . . . .	1
<b>2 Medical Background</b>	<b>3</b>
2.1 Rib Cage Anatomy . . . . .	3
2.2 Bone Fractures . . . . .	4
2.3 Bone Lesions . . . . .	5
2.3.1 Osteoblastic Lesion . . . . .	5
2.3.2 Osteolytic Lesion . . . . .	6
<b>3 Standard Reformation Methods</b>	<b>7</b>
3.1 Computed Tomography . . . . .	7
3.2 Multi Planar Reformation . . . . .	8
3.3 Rib Unfolding . . . . .	9
<b>4 Advanced Bone Visualization</b>	<b>15</b>
4.1 Programming Environment: MeVislab . . . . .	15
4.2 Overview . . . . .	16
4.3 Segmentation . . . . .	18
4.3.1 Rib Segmentation . . . . .	18
4.3.2 Vertebra Segmentation . . . . .	24
4.3.3 Artifacts . . . . .	25
4.4 Segmentation Smoothing . . . . .	26
4.4.1 WEM Smoothing . . . . .	26
4.4.2 Resampling . . . . .	28
4.5 UnwindingMethods . . . . .	30
4.5.1 Rib Clapping . . . . .	31
4.5.2 Radial Raycasting . . . . .	33

---

4.5.3	Adaptive Raycasting . . . . .	34
4.5.4	Other Non implemented Methods . . . . .	36
4.5.5	Bone Combination . . . . .	37
4.6	Slab Rendering . . . . .	40
4.7	Results . . . . .	42
4.7.1	Rib Unwinding . . . . .	42
4.7.2	Spine Unwinding . . . . .	45
<b>5</b>	<b>From Algorithm to Prototype</b>	<b>47</b>
5.1	User Interface Design . . . . .	48
5.2	Interaction Options . . . . .	53
<b>6</b>	<b>Evaluation</b>	<b>59</b>
6.1	Quantitative Comparison . . . . .	59
6.1.1	Test Cases . . . . .	59
6.1.2	Results . . . . .	60
6.2	Qualitive Comparison . . . . .	60
6.2.1	Trauma Detection . . . . .	61
6.2.2	Oncological Detection . . . . .	62
6.2.3	Evaluation Conclusion . . . . .	63
<b>7</b>	<b>Discussion</b>	<b>64</b>
7.1	Conclusion . . . . .	64
7.2	Future Work . . . . .	64

# 1 Introduction

## 1.1 Motivation

The diagnosis of the rib cage, especially the ribs, by CT data is challenging for the radiologist. The common methods need many interaction steps and have a high effort. The diagnosis with traditional planar CT images is tedious and time consuming, because the CT sections must be diagnose rib-by-rib and side-by-side. An advanced method gives the syngo CT Bone Reading, which allows to inspect ribs through straightened planar plains. This straightened ribs create a 3D data set as Curved Planar Reformation(CPR). The radiologist can diagnose the ribs, like in the multi planar reformation views, only with many interaction steps. The CT Bone Reading produces planar cutplanes, which can make the detection difficult, because the radiologist must rotate around the ribs to see them complete.

Currently it is not possible to visualize the ribs only on one 2D image. Furthermore, there is no separation from the cortical, hard bone and the spongy, soft tissue available. This separation and dimension reduction can simplify and accelerate the diagnosis of fractures and metastases.

## 1.2 Thesis Task

The aim of this thesis is the creation of a new software to assess the radiologist's detection rate of rib fractures and rib tumors in CT data. The main idea is to segment the bones and separate the bones to the cortical and spongy layer. After the separation, each layer will be unwind to get an overview of the complete structure. This representation in connection with a slab rendering reduces the image dimension into a compact 2D stack. On this stack projection methods, like maximum intensity projection(MIP), minimum intensity projection (MinIP), or average projection, can be used to highlight rib pathology. This visualization technique should support the detection rate of this pathology. Another attention of this method is the minimization of the interaction steps to save detection time and get a quicker therapy method.

The project includes the conception, implementation and evaluation of the algorithm, which visualizes the rib cage in 2D and to support the detection rate of the radiologists. The scientific contribution of the bachelor thesis includes following steps:

1. The presentation of a new visualization algorithm, which unwind the rib cage.
2. The integration of the algorithm to a Siemens Healthcare prototype. The algorithm gets a User Interface(UI).
3. The representation of a quantitative and qualitative evaluation by clinical coaches. They test the usability of the new software and compare it with the rib unfolding.

The following description of these points is divided in following parts:

Chapter 2 presents the medical background of the rib cage. It starts with the anatomy of the rib cage and follows with common pathologies. Here the rib fractures and oncological tumors are described.

Chapter 3 describes the standard diagnosis methods to find the pathologies. The sections 3.2 and 3.3 shows reformation methods based on the CT modularity to support the detection rate of the radiologist.

Chapter 4 represent the creation of the new visualization method in the MeVisLab environment. The sections describe the segmentation, smoothing and unwinding step of the algorithm.

Chapter 5 annotate the integration of the algorithm to the Siemens Frontierprototype framework. Here the Syngo.via standard is described and the design for the new method is represented. The section 5.2 represent the interaction options of the prototype.

Chapter 6 presents the evaluation of the prototype. 6.1 describes a quantitative analysis to validate the accuracy of the algorithm. In section 6.2 clinical coaches tested the prototype for usability and detection accuracy.

Chapter 7 includes an conclusion of the whole work and gives an outlook and ideas for future works.

## 2 Medical Background

### 2.1 Rib Cage Anatomy

The thorax of the human body contains 24 ribs or 12 pairs of ribs. The ribs are combined with 12 thoracic vertebrae and the sternum [7]. The combination of this bone arrangement forms the rib cage. The ribs are separated in three groups. First, there are the true ribs, which attach to the sternum by costal cartilages. The rib pairs 8 to 10 are called the false ribs, because they are not attached to the sternum. They are connected with the costal cartilage. The last ribs are called the floating or vertebral ribs, which lack anterior attachment and usually have no ventral attachment [43]. The rib bones have two types of tissues, the cortical and the cancellous bone. The cancellous bone, also known as spongy bones, is the very porous part of the rib bones end and contains red bone marrow, where blood cells are created. This is the part of the rib, which is weaker and therefore prone to fractures [35]. The cortical bone instead is very strong and dense. Furthermore, the cortical bone is the central part of the rib bones [7]. The ribs are connected with the spine, which has 33 individual bony vertebrae stacked on top of each other. The vertebrae are connected with the spinal canal and the intervertebral disc. In addition, a vertebra is composed with a body, a transverse process, a spinous process and a vertebral arch. Each vertebrae body has, like the ribs, a spongy and a cortical bone layer. The spongy layer is type of osseous tissue and is covered by a thin coating of cortical bone, which is a hard and dense type of osseous tissue [12]. The spine is divided into a cervical, a thoracic, a lumbar sacrum and a coccyx region. Each region of the spine has their own main functions, for example the cervical region supports the weight of the head. Only the thoracic vertebrae part is corresponding with the rib cage. Especially the vertebra transverse process is connected with the ribs and build a flexible connection. The main function of the thoracic part of the spine is to hold the rib cage and, in combination with the ribs, they protect the heart and lungs [37]. Also, the complete rib cage saves the stability of the human torso. A complete volume rendering technique visualization of the human thorax is shown in Figure 2.1.

Figure 2.1: VRT of the human thorax in sagittal, coronal, lateral view (From:[45]).

In clinical context rib cage pathology can appear in both parts of the bone and is divided in two common cases. One of these are trauma patients with bone fractures and the others are oncological lesions in the spongy layer of the bone. The next section describes the pathology closer.

## 2.2 Bone Fractures

Rib fractures are the most common injuries following blunt chest trauma [33]. They occur in about 10% of patients, of whom 94% have additional injuries and 12% of them are lethal. In fact, the morbidity and mortality is high. In addition, a correct rib fracture detection has a high medical relevance. To differentiate the rib fracture, they are divided in two main groups and four different fracture types. When both cortical lines were interrupted, it is called an complete fracture. A not complete fracture, where only one line is interrupted, called inner or outer cortical fracture. When the formation at the cortical line a sharp angle, the fracture is called "buckle" fracture [54]. An overview of all bone fracture types including a bone line illustration is shown in Figure 2.2.

Figure 2.2: The picture shows different bone fracture types (From:[54]).

## 2.3 Bone Lesions

Most common lesions in bones are malignant metastases and myeloma [68]. The metastases in the skeletal are osteolytic (bone resorbing) or osteoblastic (bone forming) and some are sclerotic. In many cases, there are mixed forms with osteolytic and osteoblastic characteristics [14]. Metastasis are spread parts of a main cancer [67]. For example: a prostate cancer produces bone forming lesions. A breast cancer instead can present with osteolytic lesions [44]. For a diagnosis classical features and various features are needed. Some features for the various features are the context and epidemiological details. The classical features can be the size, the type of matrix of the tumor. The localization of the lesions has an important part for the stability of the whole skeleton system and needs high attention.

### 2.3.1 Osteoblastic Lesion

Osteoblastic metastasis is usually present in prostate cancer and has a role in growing and survival tumor cells itself [14]. So, the prostate cancer metastasizes to rib bone and locally remodel the normal bone structure. This remodeling is unordered and has a disordered micro architecture, which results in a decreased stability of the bone. With this unstable structure the bone can break and consequently other parts of the body can be injured [17].

### 2.3.2 Osteolytic Lesion

The osteolytic metastases are the most common bone metastases with 75%. Osteolytic lesions can stimulate directly or indirectly osteoclastic activity and the consequence is a bone resorption [14]. Commonly breast cancer metastasis, destroys bone and they result in pain and fractures. The early phase of bone metastasis formation degrading the bone membrane. The tumor cells produce hormones, which stimulate osteoclasts. Then they proceed the bone resorption and the *circulus vitiosus* starts. The stability of the whole thorax is endangered and the consequences can be lethal [17].

Figure 2.3: The two different lesion types. Picture **A** shows osteolytic and picture **B** visualize the osteoblastic lesion (From:[30]).

Important in both cases is a correct and fast diagnosis of the pathology to choose the correct therapy method. This is very difficult with current methods because of the high number of interaction steps in each approach. The common state of the art methods, multi planar reformation(MPR) and rib unfolding, are explained in the next section.



## 3 Standard Reformation Methods

### 3.1 Computed Tomography

Figure 3.1: Overview of the CT scan and the following reconstruction method to create the resulting image (From:[23]).

In general blunt trauma patients will be diagnosed with a normal X-Ray, but often the technique has a low sensitivity so the patient will be scanned with computed tomography(CT). CT is the method, which gives answers to multiple questions with a single examination [60]. A benefit from CT to X-ray is the resulting 3D image stack. The normal X-Ray instead produces a 2D-image. The 3D data set is created by a computer-processed reconstruction of many X-Ray images from different angles to produce cross-sectional images. Therefore the X-Ray tube and the detector rotate around the human body inside the CT-tube and the resulting raw data were iteratively reconstructed and the images are created. The way from the modality to the result image is illustrated in Figure 3.1. This image allows the user to scroll through its layers, so called slices, and can use its output for diagnostical decisions. The challenge is the detection of rib pathology in the CT

dataset. Each rib has a complex shape and the course is across many CT slices [61]. Furthermore all of these slices must be evaluated rib-by-rib and slice-by-slice to get an information about all ribs to the axial slices. Mostly in oncological diseases a PET/CT image registration is used. Here the tumor cells are highlighted in the positron emission tomography(PET) and the CT data set saves the anatomy. The images are registrated by different rigid, for example rotation and translation, or with non-rigid methods, which deforms one of the image to fit it to the initial image. The two common advanced state of the art methods, by using CT images, for the detection of rib cage pathology are the multi planar reformation and the rib unfolding.

## 3.2 Multi Planar Reformation

The multi planar reformation is the most important reconstruction method for diagnoses, therapy and preoperativ therapy planning of clinical pathologies [11]. The MPR visualization of the CT dataset is the transverse, coronal and sagittal orientations of this.[53] The main benefit from MPR to the standard axial slices is that the view can combine more than one slices to a slab. This slab can be built over the axial slices. Modern software gives the reason to reconstruct non-orthogonal or obliques stacks. With a slab the diagnose of rib cage pathologies like lesions the MPR will combined with some projection methods like MIP [63], MinIP, the identical method like MIP, but there is the lowest Houndfield value represented, or average projection to highlighting them. Not only pathologies can be highlighted also bone, soft tissue can be bring in focus[11]. This MPR views was the first method to use the slab rendering. In the normal CT data sets it is not possible to combine slices.

Figure 3.2: MPR combined with MIP views of CT images. The top left image is the VRT view and the other images are the MPR views (From:[56]).

The representation includes all important views, but the problem is the slice-by-slice evaluation instead. The approach to use slabs is a better way to visualize more slices and make projection methods to them, but it is important to get an overview of all ribs on the screen. Modern software containing oblique planes can create a better display of the bone, but a new alternative must be created to get a complete overview representation of the rib cage and accelerate the detection.

## 3.3 Rib Unfolding

### Rib straightening

Kiraly et.al [27] presented a new rib visualization with a technique for tubular structure straightening by Angelelli and Hauser [1]. The technique is based on determining the centerline of the structure and then reformatting the original image space. This reformation is calculated by resampling from planes positioned orthogonally to its centerline [48]. Figure 3.3 shows an example of the straightening procedure.

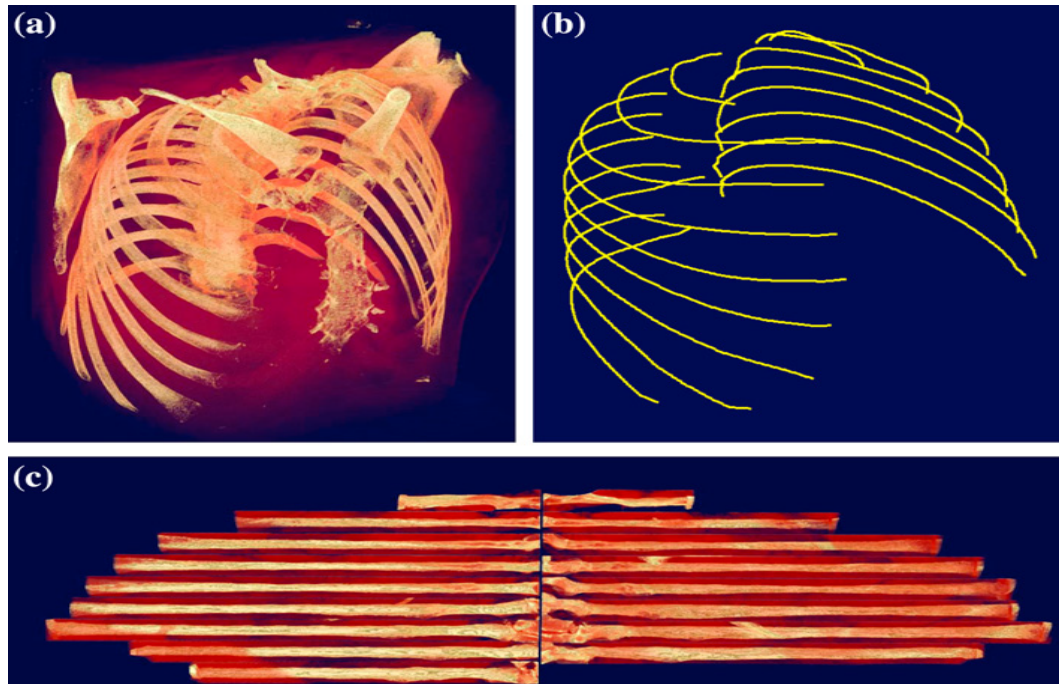


Figure 3.3: Example of the rib straightening technique. The picture **a** shows the VRT of the original CT data set. On image **b** are the extracted and smoothed centerlines and the picture **c** is a slice of the straightened data (From:[27]).

This rib straightening is a method, which enables an easier and better view of all ribs. The view enabled a better diagnosis of all ribs. The interaction steps in the standard 3D visualization and the MPR require a bigger number to the rib straightening [48]. This method was a milestone in the rib visualization, but there are many points, which can be optimized. Today the latest version of the rib straightening algorithm is the CT Bone Reading Tool in the Syngo.via Software of Siemens Healthcare GmbH.

### CT Bone Reading

To support the rib pathology detection, Siemens Healthcare GmbH in cooperation with Prof.Dr.Helmut Ringl [51] creates an algorithm to rise the sensitivity and specificity in trauma patients. The main idea was to get an overview of the whole rib cage in another representation. The CT Bone Reading application is a software, which uses CPRs for the detection of rib cage pathologies. With this algorithm the user must not slice through the standard MPRs of a dataset. Here they can rotate

around the straightened rib. To get the CPRs, the spine, ribs and vertebrae must be detected [28]. With this detection a centerline of each rib and spine is calculated [66][50] and then the unfolding algorithm starts. The visualization of the unfolded rib cage obtained by computing CPRs attached to the spinal centerline and along the rib centerlines. The whole unfolding process is visualized in the Figure 3.4.

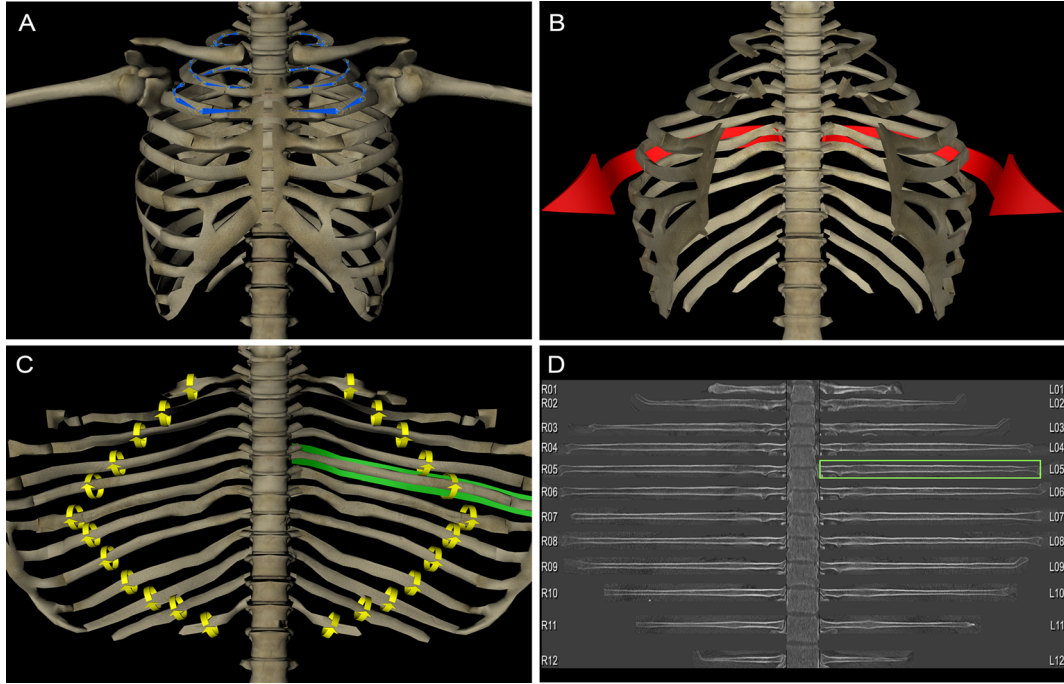


Figure 3.4: This figure shows the process of the rib unfolding **a** shows the centerline detection. Images **b** and **c** shows the unfolding. At least image **d** shows the result of the unfolding in a CPR (From:[51]).

The CT Bone Reading software creates a new representation and straightening view of the complete rib cage and found usage in trauma and oncological pathology detection. The next section concerned with an evaluation and comparison by experts from the Bone Reading against the standard MPR view detection. Relevant characteristics of the comparison are the medical accuracy and the average reading time of the fracture cases and oncological lesions.

### Rib unfolding and fracture detection

In a study by G.Bier et.al.[6] three readers were testing the MPR and the unfolded images in acquisition to sensitivity, specificity and accuracy. A big attention of the study was the reading time for each diagnosis. The unfolding algorithm reduces the reading time significantly. The sensitivity and specificity could be improved, but not significantly. Problems were created by motion artifacts. Here the unfolding algorithm gives some false positive results. However the number of missed fracture is smaller than in the 1mm-3D/ MPR view in all fracture types. An example for the fracture detection is shown in Figure 3.5 and an overview of the evaluation parameters is shown in Table 3.1.

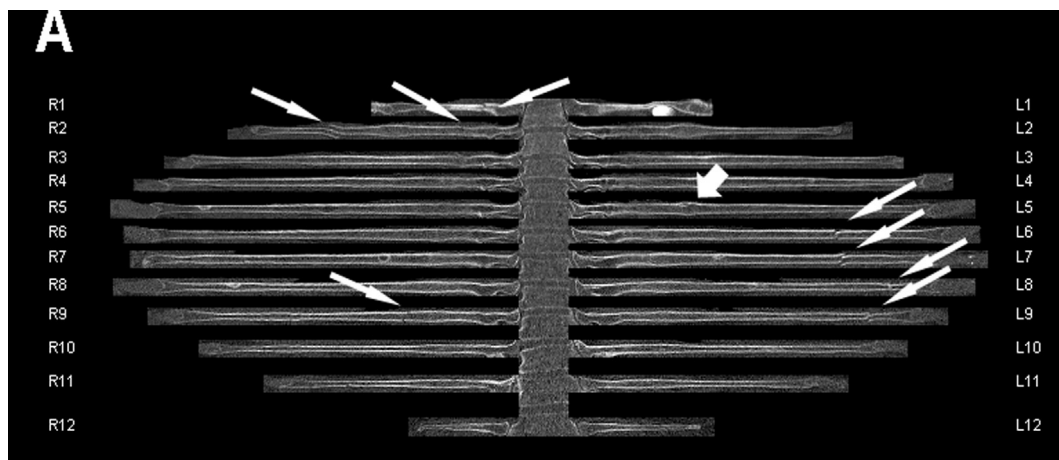


Figure 3.5: This picture shows the detection of different bone fractures in the CPR views of the Rib Unfolding algorithm (From:[6]).

	MPR			Unfolded rib display		
	Reader 1	Reader 2	Reader 3	Reader 1	Reader 2	Reader 3
Sensitivity	93.9	87.9	79.7	94.8	94.8	92.2
Specificity	97.0	97.0	82.4	87.8	85.2	82.4
Positive predictive value	99.1	99.0	94.0	96.5	95.7	94.7
Negative predictive value	82.1	69.6	53.9	82.9	82.9	75.7
Accuracy	94.6	89.9	80.3	93.3	92.7	90.0

Table 3.1: Evaluation results of the rib unfolding in trauma diagnoses (From:[6]).

### Rib unfolding and lesion detection

Homann et.al.[20] testing the rib unfolding against the standard PET/CT slice images. Therefore the typical values of sensitivity, specificity and accuracy were tested and the reading time was measured. The rib unfolding reduced the reading time significantly instead of the normal diagnosis types with 1-mm slices and 5-mm slices CT. Also the specificity and the sensitivity could be rise. The comparison is also dependent on the size classifying of each lesion. Here in both cases, lesion  $> 8\text{mm}$  and  $\leq 8\text{mm}$  the bone reading images are improved significantly against the standard CT images. The results of rib analysis is tabulated in Table 3.2 and a detection example of metastasis is shown in Figure 3.6.

Total	5 mm		1 mm		Bone Reading	
Sensitivity	47.69%		59.46%		94.81 %	
Specificity	95.65%		95.77%		88.24%	
Accuracy	0.67		0.77		0.92	
	5 mm		1 mm		Bone Reading	
	$<8\text{ mm}$	$\geq 8\text{ mm}$	$<8\text{ mm}$	$\geq 8\text{ mm}$	$<8\text{ mm}$	$\geq 8\text{ mm}$
Sensitivity	11.53%	57.14%	25.0%	73.47	89.29%	100%
Specificity	93.3%	97.5%	91.67%	97.5%	85.19%	90.24%

Table 3.2: Evaluation results of the rib unfolding in lesion diagnoses task (From:[20]).

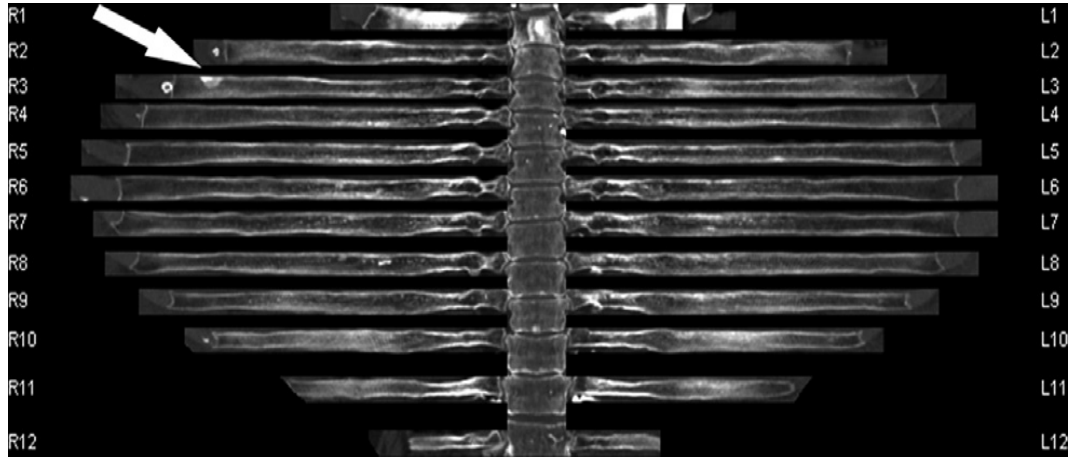


Figure 3.6: This picture shows the detection of metastases in the CPR view of the Rib Unfolding algorithm (From:[20]).

The problem of this algorithm is that the detection of small fractures and lesions is a hard task and a big number of interaction is still needed. The main idea includes only a straightening and a cut in planar planes and not to produce a complete dimension reduction of the rib cage. In fact the rib unfolding is a better reason to the MPRs, but not the perfect solution, to minimize the interaction. The rotating around the planes can be very difficult and tedious. Maybe another visualization can reduce the dimension from 3D-space to an corresponding 2D-space.



## 4 Advanced Bone Visualization

### 4.1 Programming Environment: MeVislab

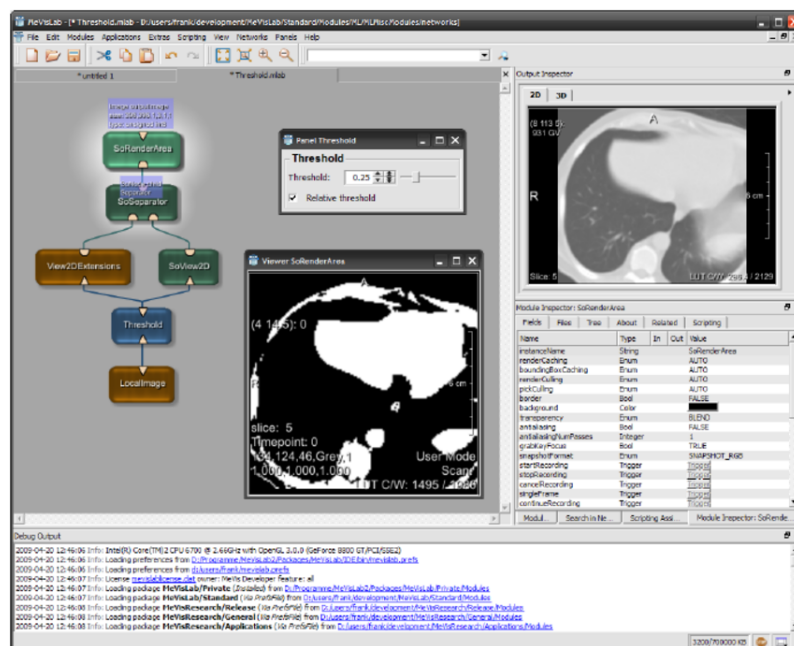


Figure 4.1: Typical MeVisLab network, which includes algorithm modules(blue), visualization modules(green) and macro modules(orange) (From:[18]).

MeVisLab is a modular framework for image processing with a special focus on medical imaging developed by Fraunhofer MEVIS and Mevis Medical Solutions AG [38]. MeVisLab includes software modules for different image processing use cases, e.g. segmentation, registration, etc. MeVisLab provided advanced medical modules for quantitative and morphological and functional analysis of medical image data. To rise the interpretation of medical relevant informations the data can be displays in two-dimensional(2D) and three-dimensional(3D) views. To develop own algorithms or applications a building of functional units(modules) are used.

They are combined with different modules and can be encapsulated into macro modules to form new parts of an application. The Figure [4.1] shows a simple network including all existing module types, which calculate a thresholding over an image. These algorithms offer the possibility to create a graphical user interface (GUI). This UI can be created by an abstract module definition language (MDL). Also, dynamical functionality is supported by scripting via using JavaScript and Python. The scripting part describes the application logic, which is the way to react on user interactions, to manipulate some algorithms or calculate and save results [18]. Besides the MeVisLab libraries developed by Fraunhofer MEVIS were external libraries for image processing tasks integrated. There are the "National Library of Medicine Insight and Registration Toolkit (ITK)" and the "Visualization Toolkit (VTK)". All of these can be combined preserve extensive processing and analyses of image data. We used the version MeVisLab 2.8.1 in combination with Visual Studio 2013, because it is the standard set up, which Siemens produce their prototypes. Prototypes are research MeVisLab application, which have the same optic like the Syngo.via application, but there are not for clinical use, only for pre-processing research tasks.

## 4.2 Overview

The "Advanced Bone Visualization" algorithm visualizes the rib cage in another way, as compared with the standard MPR and the CPR of the rib unfolding. The algorithm uses the knowledge of the centerline and vertebrae geometry by the rib unfolding algorithm. With this the segmentation of each rib will be calculated. As following steps, morphological operations are used to separate bone and spongy layer. To finish the segmentation and get the original grey values, a masking algorithm is entered. Every data set has another reconstruction and the segmented bone includes terrace artifacts. For this problem two approaches were tested and the resample approach is used for the segmentation smoothing. With the smoothed bone and centerline, the bone unwinding algorithm starts. Therefore, three different ray casting methods, with different benefits and disadvantages, are implemented. Each bone will be unwind in a loop of all steps and all the resulting rib bones are combined into one image by a concatenation algorithm. As input the user can choose between the output image size, the rib index and the using sampling method. The algorithm is divided in a rib and vertebrae part, because the segmentation steps are different. The unwind image is a compact 3D-visualization, but can compressed to a compact 2D-view by using slab rendering in combination with projection methods. This slab rendering respects the conditions

of the bachelor-thesis task of a dimension reduction. An activity diagram of the algorithm steps is shown in Figure 4.2.

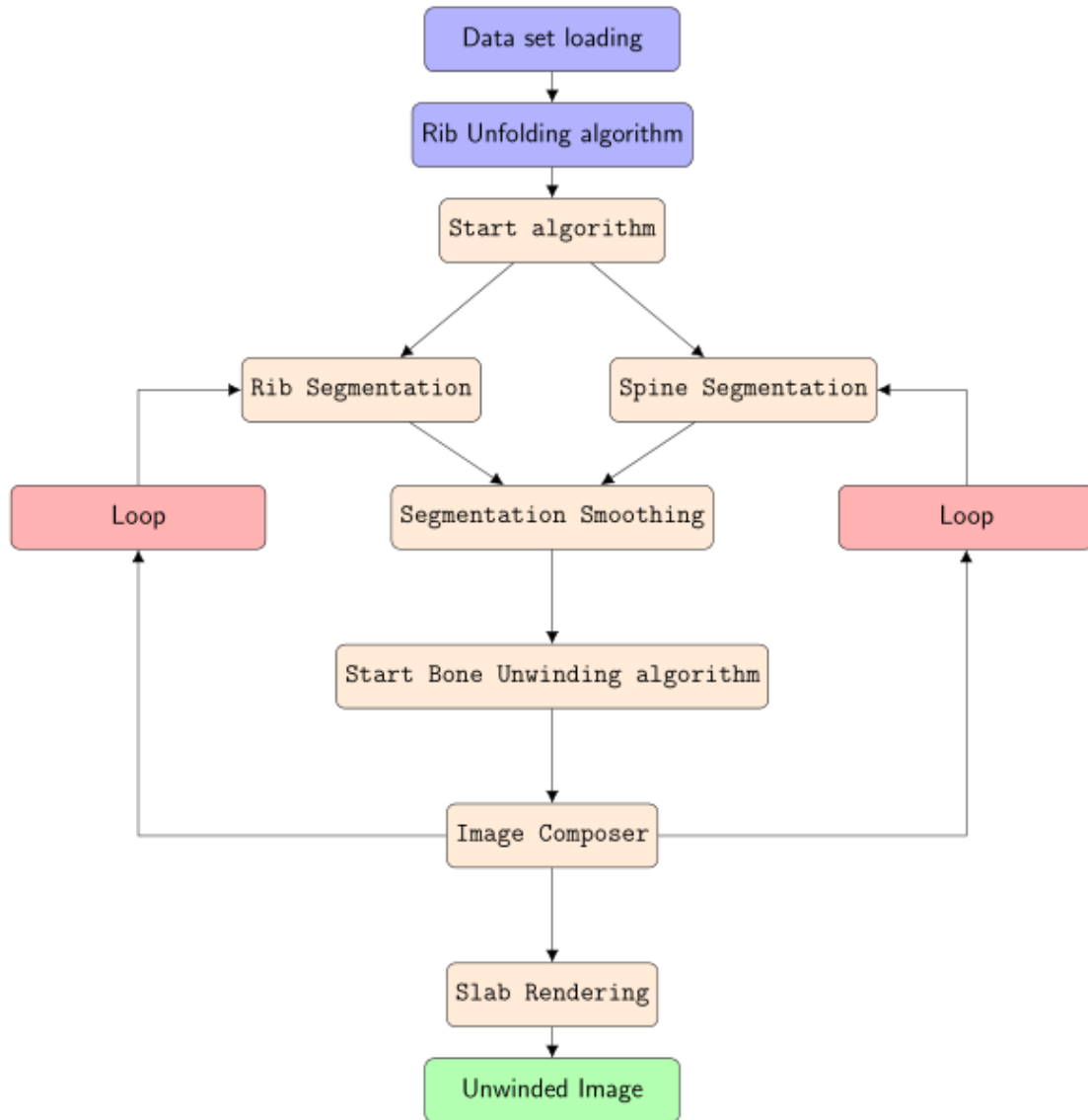


Figure 4.2: Activity diagram of the Advanced Bone Visualization algorithm workflow. Blue nodes are given parts of the algorithm and the other nodes are self implemented.

## 4.3 Segmentation

The segmentation of the rib cage is divided in two separate parts. At first the individual ribs were segmented and in the second step each vertebra. The selection of the right segmentation method is discussed by Enrico Contini [10]. In his thesis, he compared different methods for the segmentation of individual ribs or the complete rib cage. The accuracy and calculation time is an important part and a decision criterion for our approach. There are model-based, thresholding, tracing and region growing methods [50]. Because of the knowledge about the centerline points of each rib and of the spine by the rib unfolding framework, the region growing based algorithm by Lee and Reeves [31] is the approach we used for the segmentation of each rib. The centerline and vertebrae geometry submit that expensive methods, for example model-based approaches, are not valuable. Another point which qualified this approach is that CT images have a standard grey value description in Hounsfield units. In fact bones can be classified with an carefully selected threshold. Because of the grey value order, the bone can be divided in the cortical and spongy layer. The description of each segmentation step and the approaches are explained in the following section.

### 4.3.1 Rib Segmentation

The rib unfolding algorithm gives information about each visible vertebra geometry. This includes a bounding box around the vertebrae. This bounding box we use to separate the spine from the ribs. To avoid a running out from the region growing, the segmentation is divided in an "outward" and "inward rib part (Figure 4.3). The combination of both parts is realized by using arithmetic operations. The next step is the separation of the bone in two different layers. Therefore, morphological operations are used. The resulting segmentation is a binary mask. The following step is a masking algorithm to transfer the binary images from in a grey value image. This grey value image includes the values from the original data set.

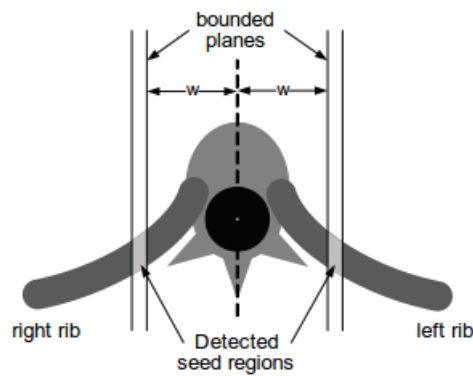


Figure 4.3: Main idea of the "inward" and "outward" rib separation by Lee and Reeves (From:[31]).

### "outward" rib segmentation

The region growing approach uses a separation of an "outward" and "inward" rib part to prevent a running out in the spine. The "inward" rib part is the region of the rib, which attached to a vertebra. To separate these two parts the preprocessed rib unfolding algorithm calculates the geometries of each vertebrae. These geometries include a bounding box around each vertebra. These boxes around the vertebrae prevent a run out in the spine, when the region growing is used. Figure 4.4 visualize the bounding box in an 2D-axial view. This image is the initial input image for the region growing. The next step is the seed point detection to segment the outward rib.



Figure 4.4: Illustration of the Bounding box around the vertebra.

The wanted seed points are the centerline points outside the spanning bounding box. The complete centerline, which was calculated by the rib unfolding framework, must be cut on the border to the "outward" rib. The aim of the segmentation is to detect the cortical bone layer of the rib. To realize this criterion, the seed points must have contact with this layer. Therefore, the points must be shifted up and down along a predefined up-vector until an average rib bone diameter is reached. After the identification of the matching points they must be add in an empty XMarkerList. This process is represented in Algorithm 1)

---

**Algorithm 1:** Algorithm for seed point detection

---

**Input:** Centerlinepoints,Bounding Box cornerpoints,rib thickness

**Output:** XMarkerList with seed points(x,y,z)

**while** *not at the end of centerlinepointlist* **do**

    get centerlinepoint;

**if** *centerlinepoint(x,y,z)inside bounding box(x1,y1,z1,x2,y2,z2)* **then**

        do nothing;;

**else**

**for**  $i = 0 ; i \leq \text{rib thickness}; i++$  **do**

            centerlinepoint = centerlinepoint(x,y,z)+

            i\*centerlinepoint.UpVector;

            add centerlinepoint to XMarkerlist;

            centerlinepoint = centerlinepoint(x,y,z)+

            i\*(centerlinepoint.UpVector\*-1);

            add centerlinepoint to XMarkerlist;

---

With the resulting list, including the seed points, and the initial image with the bounding box separation the segmentation starts. Therefore, a region growing algorithm is used. The following algorithm has a threshold parameter over 300 Hounsfield units to capture the cortical structures of the bone. Here the region is growing by iteratively adding any connected voxels in the 3D space by using 6-connectivity. After determination of the algorithm the cortical bone of the outward rib is detected (see Figure 4.5).



Figure 4.5: Segmented "outward" cortical rib bone as binary mask.

### "inward" rib segmentation

The "inward" rib segmentation is analog to the segmentation of the "outward" rib part, but here the bounding box is inverted and the seed points are the remaining centerline points inside the box. This inverted bounding box creates the initial image for the region growing algorithm. This includes the inward rib part and the connected vertebra. The visualization of this box in a 2D axial view is shown in Figure 4.6. The wanted seed points are in this case the points inside the bounding box from (Algorithm 1). Like in the "outward" rib segmentation the points must be shifted along the up-vector again to get contact with the cortical layer. The segmentation parameters for the region growing are the same, like in the "outward" rib segmentation, to detect the cortical layer of the rib bone.



Figure 4.6: Illustration of the inverted bounding box around the vertebra in 2D.

This approach is not the optimal solution for the "inward" rib segmentation, because the vertebra is inside the segmented mask, what is demonstrated in Figure 4.7. The attention of my thesis was to find a new visualization method for the rib cage. This is the reason, why the segmentation is not implemented perfectly. But in this case, we can use this approach, because the inner rib part is inside the resulting segmentation and the following algorithms are based on the centerline, so the unwinding image is complete.

Approaches for a better segmentation can be a model-based segmentation with for example a cylindrical template [31] or a gradient-based algorithm [49] to detect the rib bone without the vertebrae.

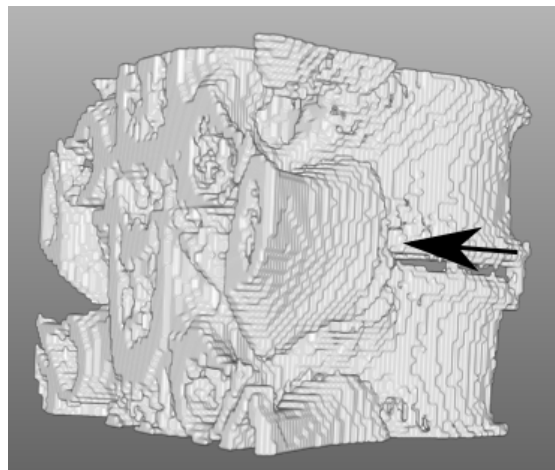


Figure 4.7: Segmented "inward" cortical rib bone as binary mask with connected vertebra.

### Connection of both parts

The "inward" and "outward" part of the rib must be combined for the further layer separation process. Arithmetic [36] image processing methods apply to use arithmetic or logical operations to two or more images. In our case, we used the logical operator OR to connect the two rib parts. This operator typically takes two images and outputs a third image, whose pixel values are the values from the first image OR the corresponding pixels from the second [16]. After this step we get the cortical bone of the individual rib (Figure 4.8). The next step of the segmentation process is the separation of the bone in the different layers, which is described in the next section.



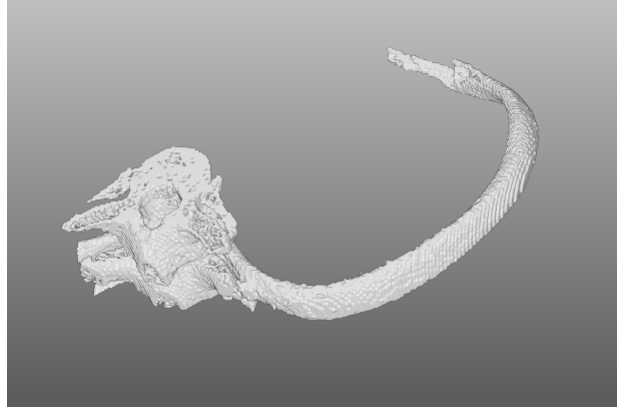
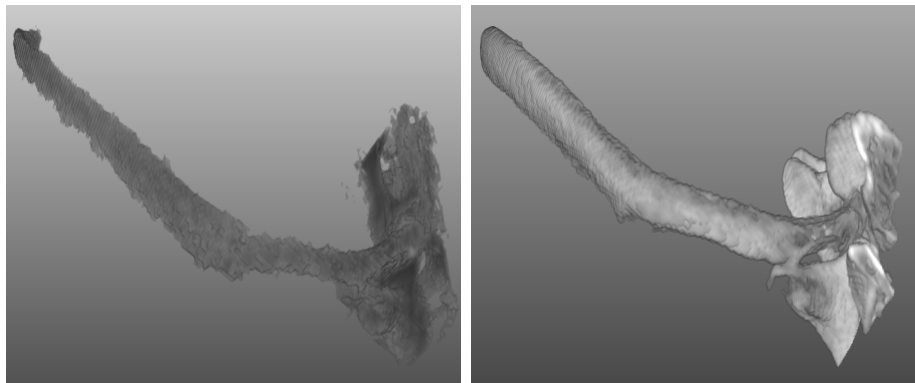


Figure 4.8: Complete connected rib bone.

### Spongy and Cortical layer separation

To split the rib into the spongy and cortical layer, morphological operations [55] are used in the algorithm. The cortical bone layer of the rib is given by the region growing. With this mask the spongy layer can be detected by using a morphological closing. The morphological closing is a special case of morphology operations and comprises a sequence of the standard operations dilation and erosion. It means that at first the structure will be close all holes by dilation and then an erosion reduces the picture, that this came near to the original structure. The closed holes by the dilation will not be opened again. The used kernel for this method is a  $11 \times 11 \times 11$  kernel to ensure a complete filling of the cortical bone.



(a) Spongy Layer

(b) Cortical Layer

Figure 4.9: Spongy and cortical layer separation with the original grey values.

The results exist as binary images, but to detect pathologies in the bones the original grey values must be recalculated. Therefore, a masking algorithm is used, which determine a convolution image, where all pixel get the original grey value, if the mask pixel has value 1. The different segmented structure from the cortical and spongy layer will be masked with the original data set.

### 4.3.2 Vertebra Segmentation

The segmentation of the vertebrae proceeds like the rib segmentation. In this case the bounding box of each vertebrae is used to separate the spine from the complete data set. As seed points for the region growing the spine centerline from the rib unfolding framework are used. The spine centerline points were tracked by Kalman filtering [25] through the consecutive 2D spine cross-sections [50]. Again the region growing method is used with a thresholding parameter of 300 Hounsfield units.



Figure 4.10: This image displays the segmented vertebra in 3D.

The separation in the cortical and spongy layer is not possible, because the grey value distribution is too noisy to calculate a good threshold. A problem is the fibrous spongy layer in the vertebra body, which produces cortical bone parts. This cortical bone parts were transported over the fibrous structure. This fiber is very dense and in Hounsfield units it is nearly the same as the outer cortical bone. Another point is the included segmentation of the "inward" rib. The connection between the transverse process and the rib bone results a run out in the rib bone. But here again the result is usable, because for the unwinding algorithm, all structures are detected, which are important.

### 4.3.3 Artifacts

After the segmentation process the voxel structure of the rib shows terrace artifacts (Figure 4.11), which produce many problems in the following unwinding algorithm. These artifacts emerge in the reconstruction of the CT raw data to the viewing data [19]. The reconstruction is limited by the pixel matrix of the output image. So mostly the raw data are too sharp for the pixel matrix or the available pixel are too small [13][3]. The artifacts must be reduced by a carefully selected smoothing technique. A filter method is not an option, because the manipulation of the original grey values is too strong. For example, little fractures will be neutralized by filter algorithms like Gaussian filter [8]. Even an edge-preserving filter like a median filter [22] manipulate the grey values too huge.

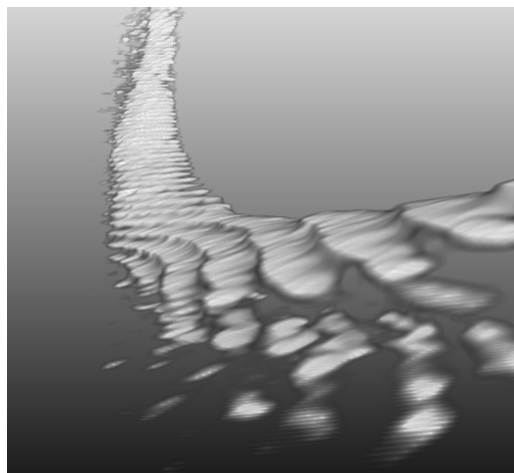


Figure 4.11: This picture shows the terrace artifacts of the rib voxel structure.

In the next part, we present two approaches to smooth the segmented rib structure. The algorithms only must be used for the rib bone, because the vertebrae segmentation not contains the artifacts or they are too small. Consequently the vertebra segmentation can be ignored in the smoothing step.

## 4.4 Segmentation Smoothing

A good smoothing method fulfils many requirements derive by Bade et. al. [3]. The smoothing must reduce the artifacts and should not increase existing artifacts or create new artifacts (1). Topological failures can be ignored, because the segmentation and the following morphological operations restore a connected and continuous diameter characteristic. The next point (2) is the accuracy of the smoothing. Therefore, the smoothing must preserve the volume, the form and the distances between neighbor points. In this case spatial extensions and relations must be conserved. The last point (3) is the practical application of the smoothing algorithm. The parameter setting should be very easy or automatic, for example: a carefully selected default value can be use. In addition, the algorithm must be stable, when different parameters are used and should not influence the performance. The smoothing need a good duration time to find usage. Time in medical diagnosis context is important for therapy possibilities. [2].

Criterion	Requirement
<b>1.Smoothing</b>	1.1: Reduction of block artifacts 1.2: Reduction of terrace artifacts 1.3: Correction of topological failures (holes, ...) 1.4: No increase of existing artifacts 1.5: No creating of new artifacts
<b>2.Accuracy</b>	2.1: Preservation of volume 2.2: Preservation of form 2.3: Preservation of distances
<b>3.Practical Application</b>	3.1: Easy/automatic parameters 3.2: Efficient runtime

Table 4.1: Overview of smoothing requirements in medical context [2].

The table 4.1 represent all requirements in an overview, which observe the choice of the best smoothing method for the segmented rib bones in the next part.

### 4.4.1 WEM Smoothing

The first approach we investigated, was a mesh smoothing. Therefore, an iso surface of the rib structure must be created. This mesh must be retransformed to an image mask to get the grey values of the original data set, to detect rib

pathologies. To create a surface of the segmented rib bone the Mevis winged edge data structure is used [5]. This is a powerful structure by using marching cubes [34] to transfer the image into a triangle mesh. The WEM contains a pointer of each edge with the two corner points and their adjacent faces and a second pointer, which includes the accessor and the successor edge in two faces. A benefit of using this data structure is the fast access of the neighboring structures for the following smoothing algorithm.

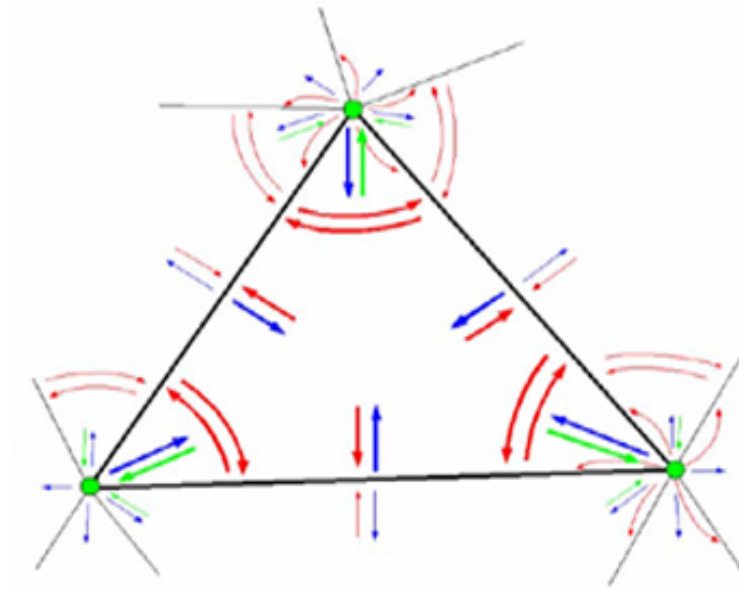


Figure 4.12: Visualization of WEM-pointerstructure, if both pointers are connected (From:[38]).

The structure of most bones is elongated. Furthermore bones have no branches, like a vessel tree and in this case Taubins LowPass [59] or Laplace+HC [62] filter are possible methods to the smooth bones [3]. The simple and low parameterized Laplace or Mean filter are worst to use, because the volume shrinking is too strong [4]. The Laplace+HC and LowPass filter confirmed the requirement for a little number of parameters and there are automatic methods [39]. For testing purposes we used the Laplace+HC filter with 10 iteration and a factor of 0.5. The result is shown in Figure 4.13.

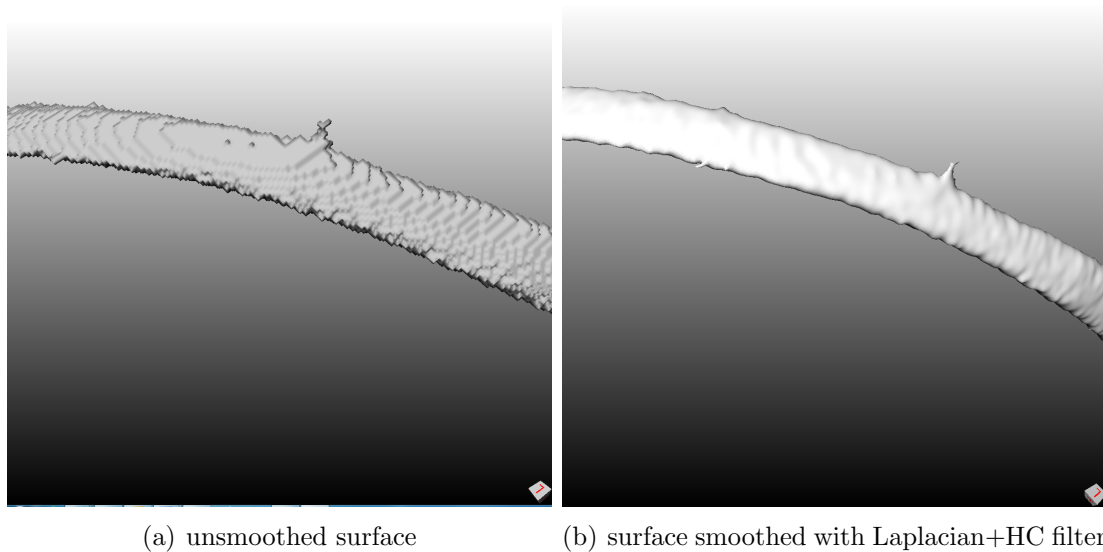


Figure 4.13: Illustration of the smoothing result.

The calculation of the smoothed rib structure is efficient and reliable. The artifacts can nearly completely be deleted from the structure and the volume preservation is given. The method seems a good approach, but it cannot be used for the following steps, because the original grey values are needed and the recalculation from the mesh grid to a voxel grid [21] creates the terrace artifacts again. Consequently, another smoothing method must be found to smooth the artifacts in the rib segmentation.

#### 4.4.2 Resampling

The next idea to smooth the artifacts is resampling. Resampling is a mathematical method to change the image size in different height and width. That can be an upsampling, which increases the size of the image. A reducing of the image size is called downsampling. To smooth the rib segmentation upsampling is requested to reduce the terrace artifacts. This method uses an interpolation between the existing pixels to get the values at the new pixel locations. Possible interpolation techniques in this case are the cubic [26] and the lanczos [15] interpolation. Important is a good trade-off between accuracy and speed. After testing with different data sets the cubic interpolation method finds use in the resampling with the scale factor is 3 in x, y and z-direction [65]. The result, which is shown in Figure 4.14, shows an image with reduced artifacts.

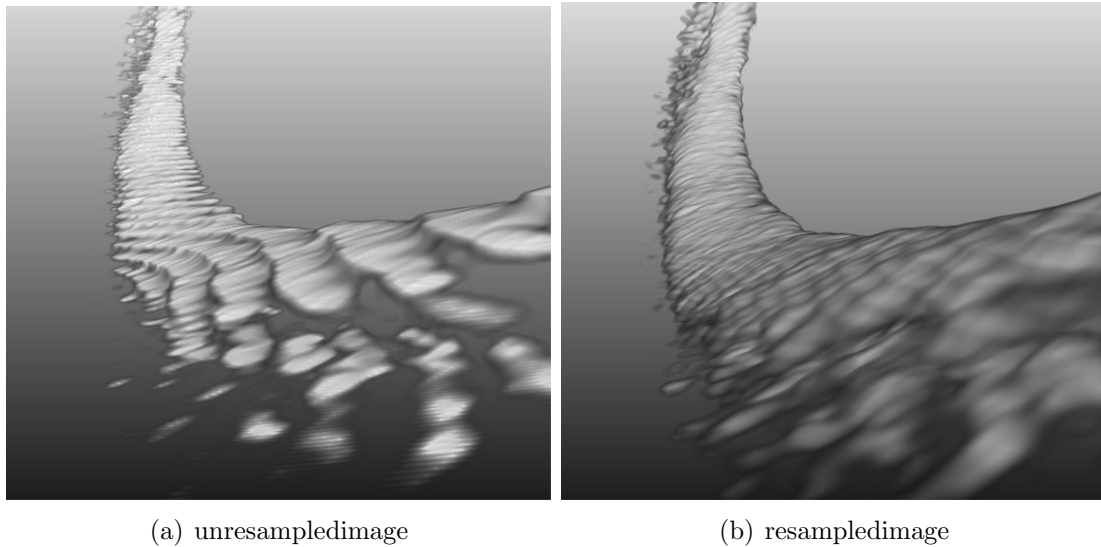


Figure 4.14: Comparison between the normal rib voxel structure on the left side and the resampled image on the right side.

This approach smooth the terrace artifacts satisfactorily. Because of the interpolation between the original grey values its emerge a minimal blurred image. However, in this case it can be ignored, because the more important part of the artifact reduction get a higher significance and the resulting grey values come close to the real values. With this smoothed bone the unwinding algorithm can start. The different implemented unwinding methods are explained in the next chapter.

## 4.5 UnwindingMethods

In this section the segmented and smoothed rib will be unwind by different methods, which visualize the rib in another way. The approach creates a new image transformation technique for the rib. In all implemented methods, a raycasting [64] algorithm is used to sample the original rib voxel and transform them to the new image space. The sampled points of each ray in general are not aligned with the volume and they will usually be located in between voxels. For this reason, it is necessary to interpolate between the surrounding voxels. Therefore, we tested the common interpolation method trilinear and tricubic interpolation. The trilinear interpolation is a sequence of linear interpolations in the 3D-space [29]. More accurate results are achieved with the cubic interpolation approach, which calculates a continuity between 4 following voxels [32]. The duration time is higher in the cubic interpolation and after a few test samplings the trilinear interpolation method gives a better trade-off between performance and quality then the cubic interpolation.

### Raycasting

The standard raycasting method is a technique to visualize three-dimensional volumes of image data. The main idea is to generate initial rays for each pixel of the image plane and trace their intersection with the volume. During the tracing sample points in regular distanced were defined, which described the opacity and color values along the ray. In the last step, these values will be combined and the resulting pixel values can be calculated in the image space [52].

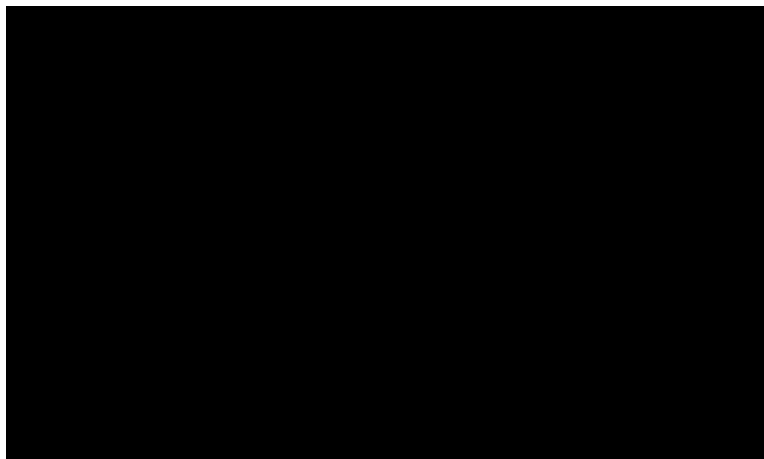


Figure 4.15: Illustration of the standard ray casting method.



The ray casting algorithm we used is different to the standard. In our approach the volume will be sampled along the ray and the resulting image is a compact 3D image stack. Consequently, the difference is that the ray sample will not be accumulate to one value. Here each sample will be listed in the resulting image stack. Each unwinded image has another sampling order and consequently another visualization. The image stack size and using sampling order is certain by user input values.

### Input values

As input the algorithm needs a segmented bone and the centerline. To rotate the ray around the centerpoint the up vector will be defined. Because of the ray sampling approach, it is important to reconstruct the original data set in an ideal way. An undersampling or oversampling of the bandlimited signal should be avoid, because it leads to aliasing artefacts. These artifacts would bring disturbances in the resulting image. Nyquist Shannon sampling theorem describes that a bandlimited signal, in our case the segmented bone must be sampled with a frequency greater than the double signal, that the signal will exactly and determine reconstructed [42]. To secure observance of the theorem the centerlinepoints will be upsampled, such that two centerline points are inside one voxel. The user input contains the operating sampling method, the resulting y-size and z-size of the unwinded image, the layer selection and the option to unwind the ribs. For the unwinding methods only the image sizes and the chosen method is decisive.

$$f_{sampling} = 2 \cdot f_{max} \quad (4.1)$$

#### 4.5.1 Rib Clapping

The first approach is a parallel grid sampling and a visualization of two halves of the bone. The rays trace the upper and lower half of the bone in a parallel grid. The z-size input of the user described the sample size in depth of the sampling. The half number of the depth will sample the lower half and the other numbers of depth points sample the upper half of the bone. The parallel traced rays on each z-step describe the y-dimension of the resulting image. To displace the complete rib regions in the image each parallel half ray get 25% of the y-input. The illustration of this method and visualization of the resulting image is shown in the following figures 4.16 and 4.17.

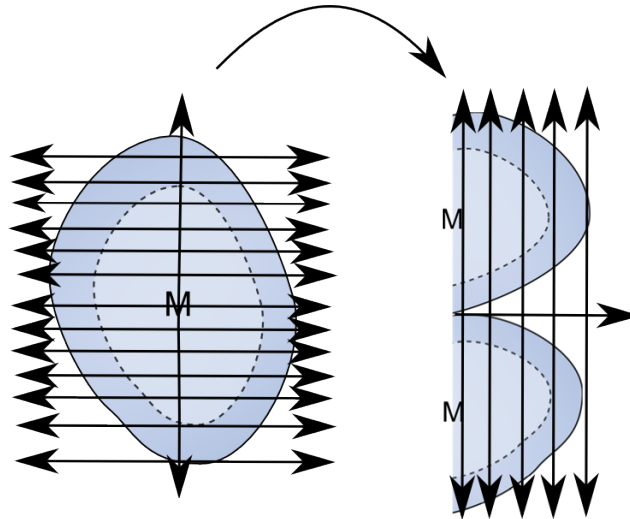


Figure 4.16: Illustration of the rib clapping approach.

### Resulting image stack

The resulting 3D-image stack shows the two rib halves from the inner tissue to the outer rib. The x-axis contains the centerline point length. The y-axis shows the upper and lower half of the rib and the z-axis goes from the centerline point, which is in the center of the rib, to the outside of the bone.

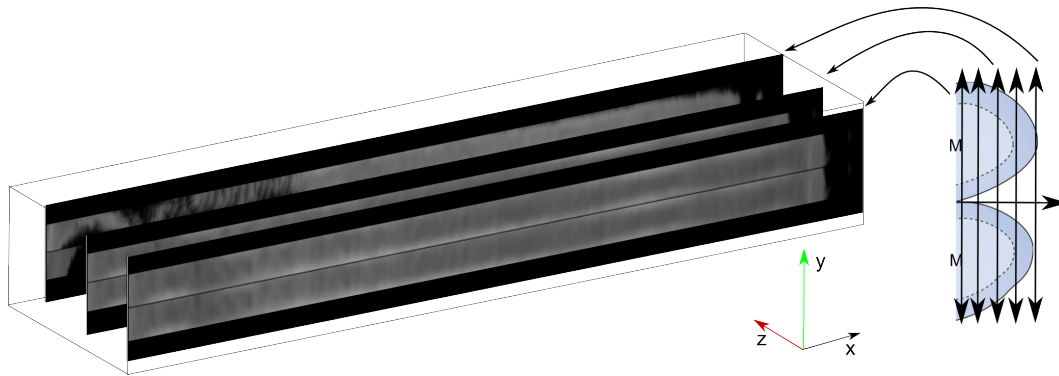


Figure 4.17: Illustration of the resulting image stack by the rib clapping method.

## Benefit and Disadvantage

This approach is free from segmentation artifacts, because this method creates only a cut the bone in planar areas. This characteristic is a benefit, but the problem is the unintuitiveness of the resulting image. The representation of the upper and lower half of the bone at the same time may seem that one rib will be divided into two ribs. This criterion is crucial for searching a new intuitive representation of the rib bone.

### 4.5.2 Radial Raycasting

The second approach is a radial sampling unwinding. Here the sampling points are ordered in concentric circle. The centerline points build an axis to the next and then a corresponding up vector is defined, which is the rotating vector. The rotation is axis-aligned and the sampled angle is dynamically calculated based on the user input. The number of circles is the depth input of the user. The maximum distance of the ray is limited by an average maximum rib thickness. Consequently, each depth input is fitted on the average thickness. This method is illustrated in Figure 4.18 and the resulting image stack is shown in Figure 4.19.

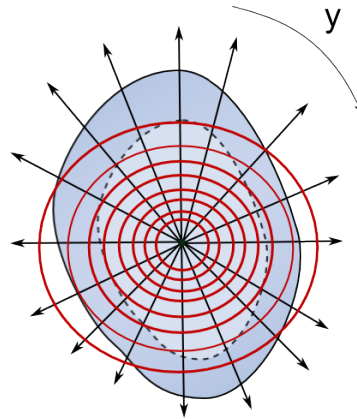


Figure 4.18: Visualization of the radial sampling method

## Resulting image stack

The resulting image stack is different to the clapping algorithm. Here the z-axis describes each concentric circle from the middle of the bone to the outer bone. All

sampled angles are added to the y-axis. The x-axis includes again the center line points.

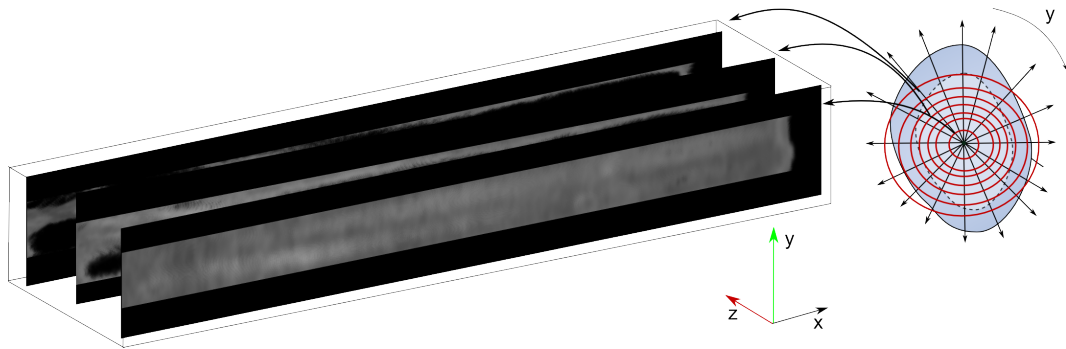


Figure 4.19: Illustration of the resulting image stack by the radial raycasting method.

### Benefit and Disadvantage

This method included the size relationship to the original data set, because of the concentric circle sampling. The visualization is consistent and the interpretation is more intuitive compared to the clapping approach. The disadvantage of this method is the elliptical form of a bone, especially the rib bone has a nearly exact elliptical structure. In the illustration of this method in Figure 4.18 the concentric circle are outside the bone on the thin part. In the resulting image these areas are dark regions in the picture. The information density in the unwinded image is certainly not satisfactory, that some information in the result is wasted in elliptical bone cases. In the vertebra body case, which form is more circular, this method is good and can be use, because the sample points outside the bone is low.

### 4.5.3 Adaptive Raycasting

A better way to respect the elliptical bone structure is a dynamic ray casting approach. This method has nearly the same behavior like the radial sampling method. The difference in the third approach is an adaption of each traced ray to the current bone structure. First, each ray is traced, until it leaves the bone. This rib length will be saved for each angle and each sampling point is adapted to the ascertained ray length. Consequently, the resulting slices in the unwinded image are the bone form. The following figures 4.20 and 4.21 illustrate this method.

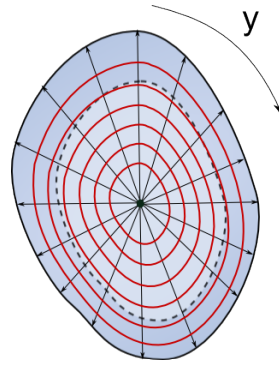


Figure 4.20: Visualization of the adaptive rib casting.

### Resulting image stack

In general, the generated image stack, which is created by the adaptive raycasting method, is the same like in the radial method. The huge different is the combination of the y-axis and z-axis. Here again each angle is filled on the corresponding unwinded image, but each slice is not a concentric circle on the z-axis. The difference is, that each slice is described by the bone structure and represents this structure.

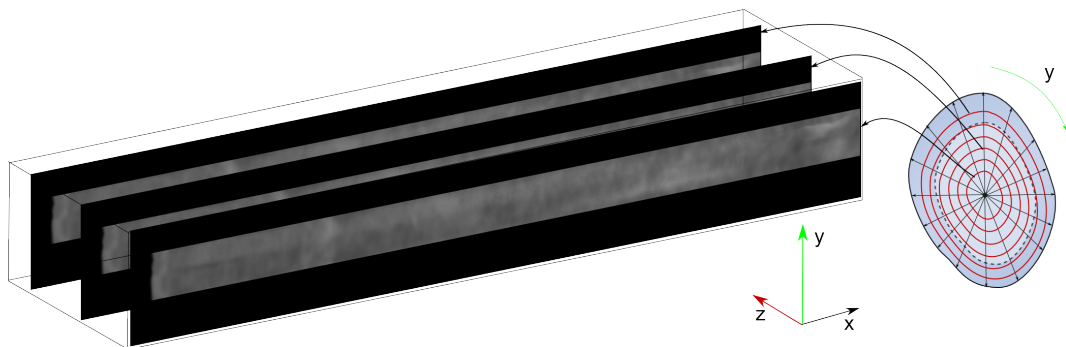


Figure 4.21: Illustration of the resulting image stack by the adaptive raycasting method.

### Benefit and Disadvantage

In fact, the compliance to the bone structure in the unwinded image use the information density of the resulting image optimally and seems as the best method to unwind bones. A small disadvantage is the navigation in the new image space

compared to the original data. The interpretation and connection is quite difficult and should be supported, for example: by a synchronized recalculation from the unwinded image to the original data space, combined with a user interaction via reference lines. This interaction option is explained in the next chapter *Algorithm to Prototype*.

#### 4.5.4 Other Non implemented Methods

In the design stage more methods are created but find no usage in the algorithm, because of different reasons. Two more ray casting methods are described in these parts and the rejecting reason for the non-implementation will explained.

##### Standard Rib Slicing

We considered an approach that not "unwind" the bone structure. Here the idea was to sample the complete rib and fill the image in the way, that the slicing goes from the bottom of the bone to top. The reason, why it found no usage in the prototype is the following combination with the slab rendering and connection with projection methods. With a slab the complete rib is composite and the use of a MIP only highlights the bone and a detection of for example osteoblastic lesion or other pathology is impossible.

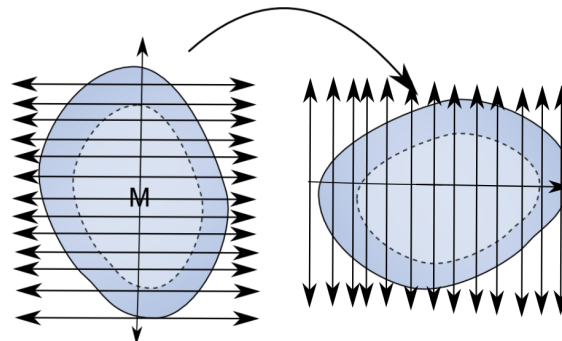


Figure 4.22: Illustration of the standard Rib Slicing approach. The resulting image stack scrolls from the bottom to the top of the bone.

##### Spiral Ray Casting

Another approach was a complete dimension reduction of the 3D-image space to an 2D-image space. The idea is a spiral ray casting method. For each angle ray

the length must be fitted to the correct bone structure. Then the ray will be sampled along an adaptive spiral form around the bone. The resulting image has only an x-axis, which includes the centerline, and a y-axis, which describes the sampled points. The main idea of an dimension reduction is inserted, but with this representation approach a detection is very difficult, because if a patient has a partial fracture, means many points on the y-axis occurs and it seems that there is more than one fracture. Because of these reasons the approach find no usage in the prototype.

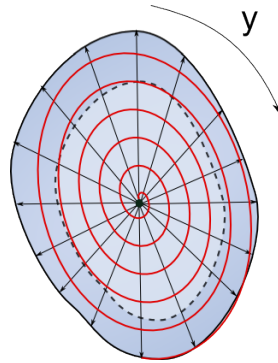


Figure 4.23: Illustration of the spiral sampling approach. The resulting image stack describes the straightened spiral.

### 4.5.5 Bone Combination

#### Rib Combination

The algorithm unwinds one input bone. If the user wants to get an unwinded image of all ribs, each rib must be combined in a new image. Here an image composing algorithm is used, which provides operations to concatenate an image to an existing volume at a user-defined position. Because of the knowledge about the rib index, the rib number, the direction of each rib and the corresponding vertebra, the algorithm pipeline can run iteratively for each rib. The image composing algorithm calculates the right position for the unwinded rib image. The z-position in all cases is the first slice to synchronize the slicing process and all slices have the same depth. The schematic visualization of the image composer is shown in Figure 4.24. The two parameters, which must be calculated is the x- and y-coordinate.

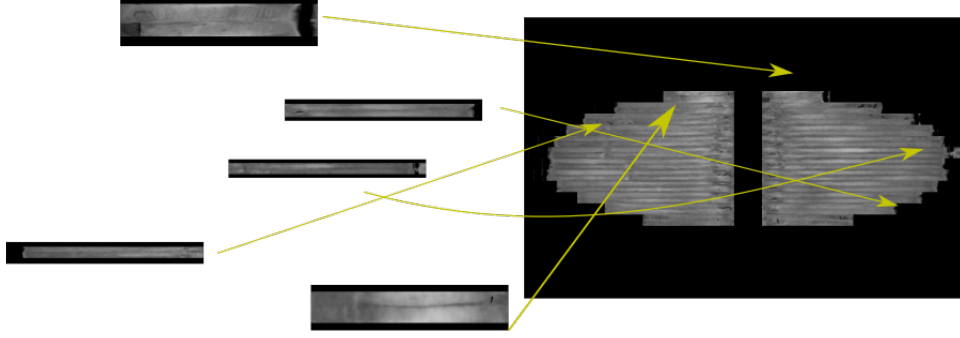


Figure 4.24: Schematic visualization of the rib image composing calculation.

The x-coordinate is calculated by a fixed constant value and centerline length of the bone. The anatomy of the human describes a left and a right part of the rib cage. With the knowledge about the rib directions and rib indices from the unfolding framework, the unwinded rib bones can correctly ordered. If the rib index is greater than the half rib number, the side of the rib is left. All other ribs are on the right side. In this case the ribs are fitted on the value 1700. This fixed value is chosen by many test cases to detect the average maximum centerline point number. To save the length relationship from each rib, the x-size of the individual bone is subtracted to a fixed value of 1500 for ribs on the left side. This two cases describe the x-position of each unwinded rib bone in the image composing algorithm.

$$posx_{unwinded} = \begin{cases} 1700, & \text{if } ribid < ribnum/2 \\ 1500 - centerlinepoints, & \text{otherwise} \end{cases} \quad (4.2)$$

$$(4.3)$$

With the correct x-coordinate the bone would be overlap in the image composed image. The next step is the calculation of the y-position of each individual rib bone to save a correlation to the human rib cage. Again, the knowledge about the rib indices and maximum rib number by the unfolding framework is used. Important for the y-position calculation is the user input about the angle samples. This input must be dynamically adjusted to the resulting composed image. If the rib index is again smaller than the half rib number, the y-position determines by a multiplication of the current index and the input y-size by the user. Otherwise the rib index must be subtracted with the half rib number to fit the correct rib pairs together.

$$posy_{unwinded} = \begin{cases} ribid \cdot inysize, & \text{if } ribid < ribnum/2 \\ (ribid - ribnum/2) \cdot inysize, & \text{otherwise} \end{cases} \quad (4.4)$$

$$(4.5)$$



## Vertebrae Combination

The unwinding vertebrae algorithm branch is nearly the same like the rib bone unwinding. The vertebrae will unwind individual and must be fitted in a resulting image, which includes the vertebrae on the right position. The right position means the observance of the spine vertebrae order. The chronology of the algorithm processes is from the highest vertebra to the lowest. Consequentially the vertebrae will concatenate on the x-axis. This resulting image of the resulting unwinded spine is shown in Figure 4.25.

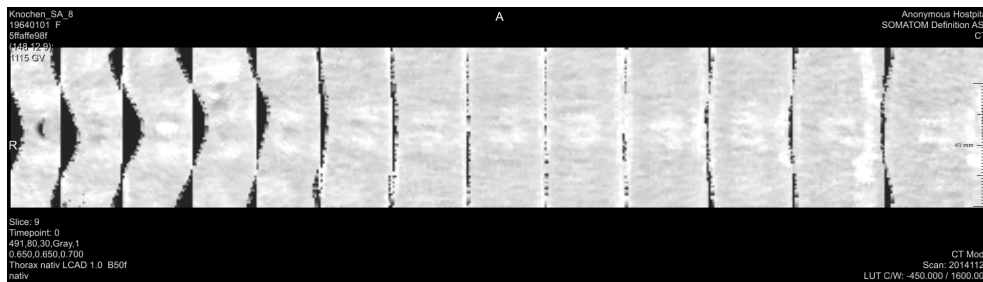


Figure 4.25: Illustration of the resulting image stack by the adaptive raycasting method.

## 4.6 Slab Rendering

For diagnostic tasks with CT data, a slab rendering is an accepted method. This method involved a stack of slices to represent them on the screen[47] [46]. The resulting image stack of the ribs need a slicing from the middle to the outside of the rib. The aim of the bachelor-thesis is to minimize the interaction steps. Consequently, a slab rendering in combination with the typical projection methods is realized. The projection methods should highlight typical characteristics of bone pathologies. For example: to highlight an osteoblastic lesion in a bone, a minimum-intensity-projection is employed, because the main property of this lesion is the bright grey value. The opposite is the osteolytic metastasis [40]. They have darker grey values and a maximum-intensity-projection can be used to intensify the neighboring healthy structures. To identify normal properties of bones, an average projection is a good choice [41]. The slab rendering can be used for all unwinded layers. The benefit of this method is that the complete bone surface is represented in one view and can be diagnosed instantly and the large number of interaction steps are reduced. The following Figures 4.26, 4.27, 4.28 show a trauma data set with a slab rendering over all slices and all three projection methods. The circles show the different representation of the same partial fractures.

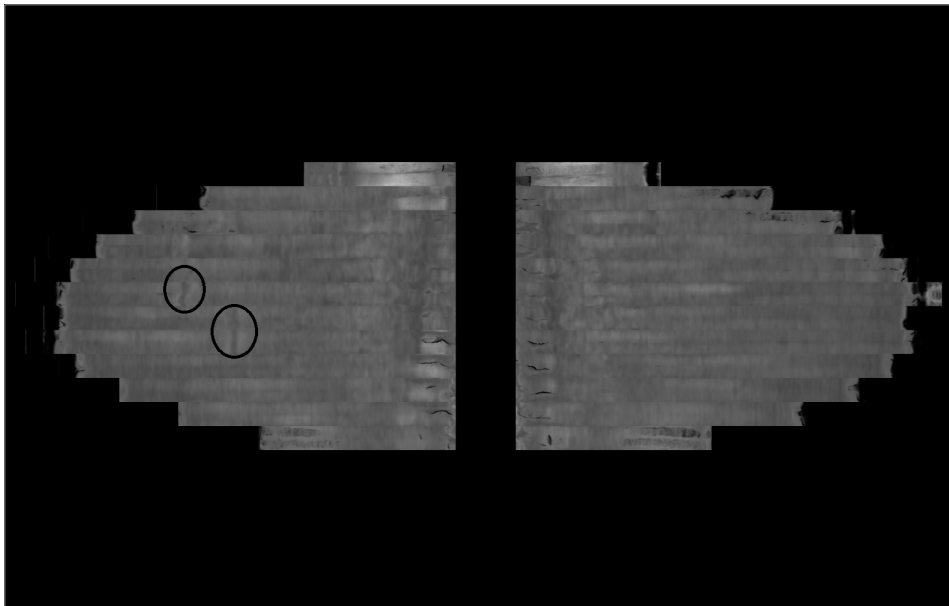


Figure 4.26: Display of the unwinded image with a minimum intensity projection. The encircled regions show rib fractures.

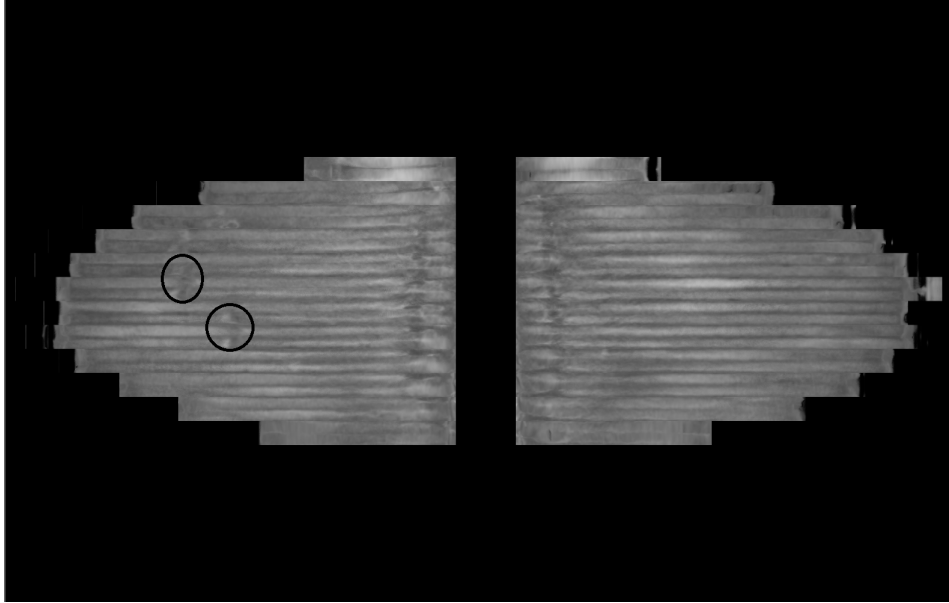


Figure 4.27: Display of the unwound image with a maximum intensity projection. The encircled regions show rib fractures.

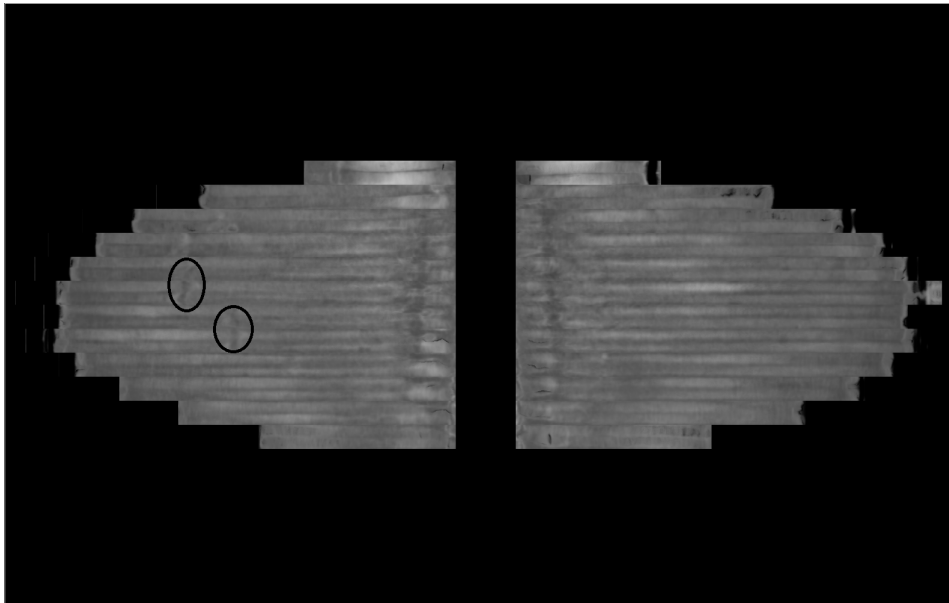


Figure 4.28: Display of the unwound image with a average projection. The encircled regions show rib fractures.

## 4.7 Results

### 4.7.1 Rib Unwinding

#### Trauma Case

The following unwinded images show some possibilities of the unwinding algorithm for the ribs. The first image shows a fatal trauma data set with many complete fractures. The unwinded image in combination with a maximum-intensity-projection (Figure 4.29) enhanced the healthy bone and the fracture can be detected well, because the fracture is dark in the image. The black stripes in the inward rib can be explained by bounding box and centerline failures from the rib unfolding framework.

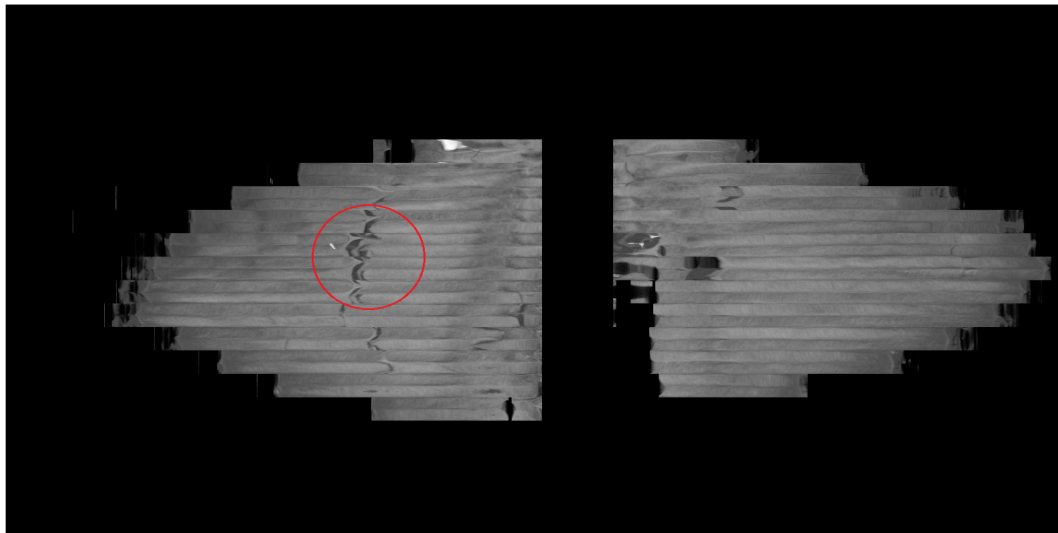


Figure 4.29: Slab rendered unwinded image of many complete fractures. The black block on the right shows artifacts, because of missing centerlines.

A more complicated detection task relates to incomplete and "buckled" fractures. The characteristics can be very bright on the buckled fracture and the partial fracture can have both properties. One half of the rib is bright and the other half in the bone is the fracture part and has dark grey values. Therefore, it is useful to check the image with maximum and minimum-intensity-projection to categorize the existing pathology. The following data set includes some partial and "buckled" fractures, which are enhanced by slab rendering. (see Figure 4.30)

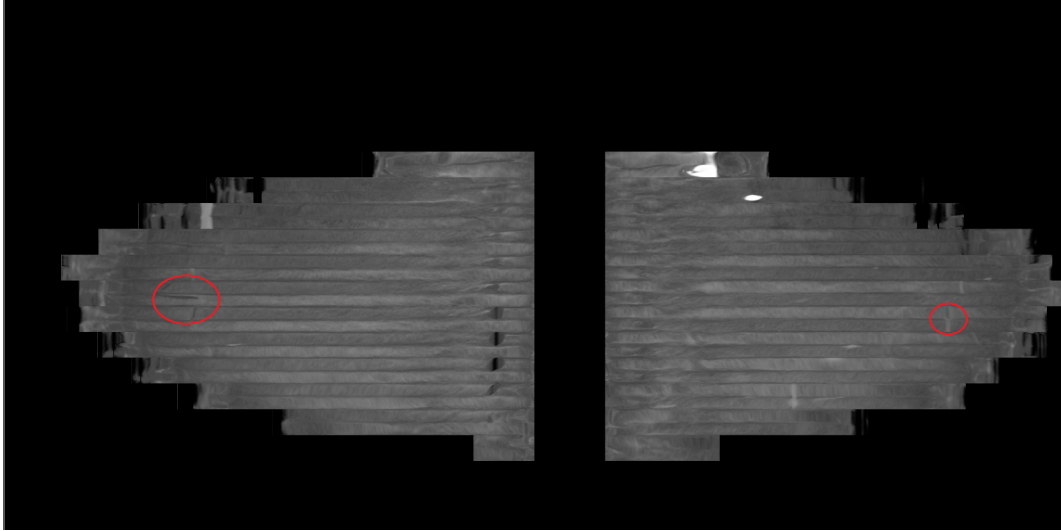


Figure 4.30: Example for partial and buckled fractures in an unwound image.

Another option to detect fractures is to unwind only the cortical layer of the bone. The option of layer separation gives a representation of the cortical bone only. Some disruptive structures of the spongy layer are deleted and the point of view is on the bone. An example is shown in Figure 4.31.

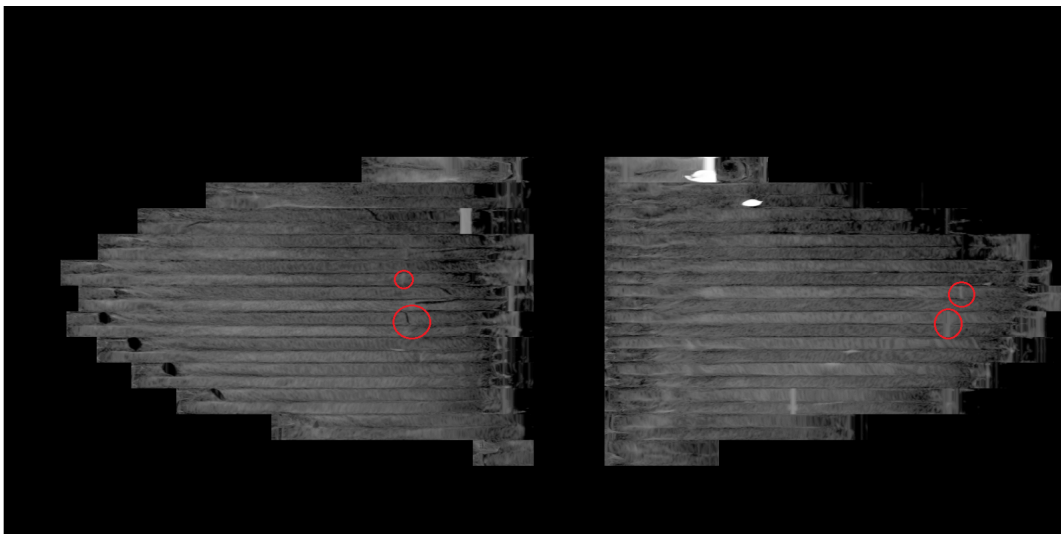


Figure 4.31: Unwound cortical layer of different partial fractures.

### Oncological Case

Another clinical case is the detection of oncological lesions and metastasis. In this case, it is necessary to highlight them by using maximum- or minimum-intensity-projection. A combination of the unwinded image and slab rendering techniques make it possible. An example for an osteoblastic lesion is displayed in Figure 4.32.

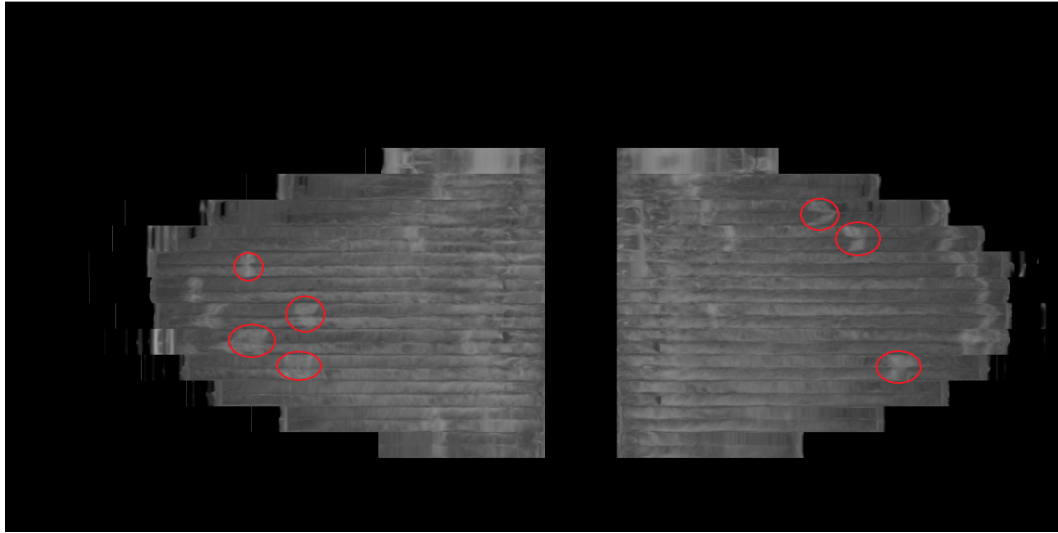


Figure 4.32: Example MIP to highlight osteoblastic lesions in the ribs.

A problem can be the cortical bone structure. With a maximum-intensity-projection the bony structure comes to the foreground. Therefore, the separation into the spongy layer delete the cortical part and unwind only the pathology soft tissue. If here a MIP is used, the osteolytic lesion is highlighted. By using an MinIP in the slab rendering, osteoblastic metastasis are shown. An unwinded image of the spongy bone layer is shown in Figure 4.33.

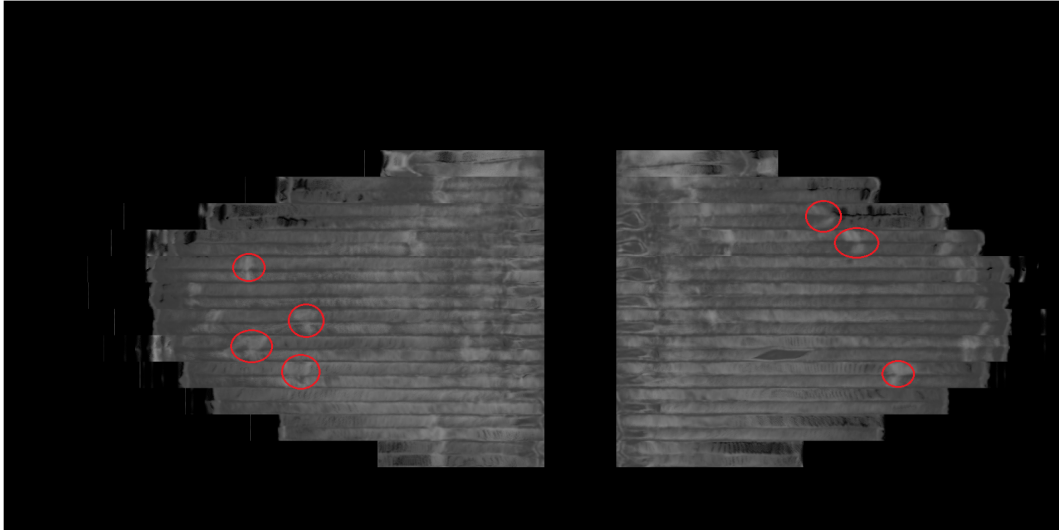


Figure 4.33: Example unwinded image of the spongy layer.

### 4.7.2 Spine Unwinding

#### Trauma Case

This section shows results of the algorithm for the spine in the trauma and oncological case.

The unwinded image for trauma patients shows fractures by dark grey value regions. On these regions, the cortical line is interrupted and there are holes. Deformed vertebrae are shown good, because the surface is direct represented in the unwinded image and the form.

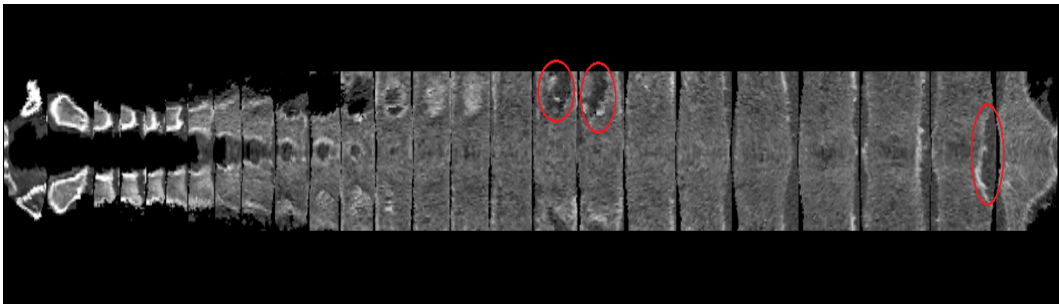


Figure 4.34: Unwinded spine with fractures.

### Oncological Case

The spine unwinding in combination with projection method highlights the metastasis lesions. A problem is the missing separation of the cortical and spongy layer. The projection method highlight in this case not only the osteoblastic lesion. However, by choosing a smaller slab size of the inner part only the lesion and spongy layer can be projected.

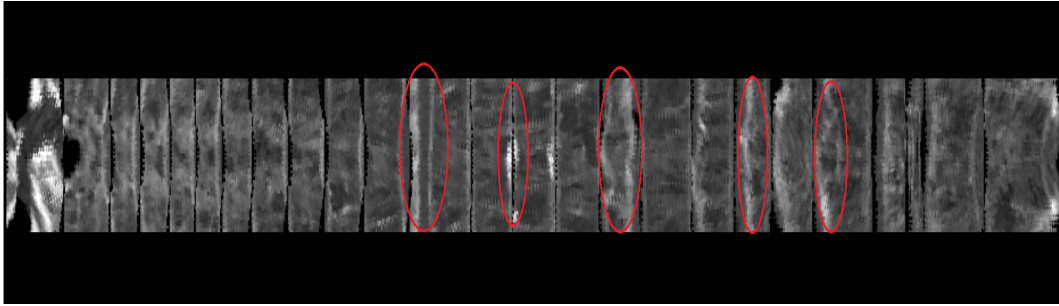


Figure 4.35: Unwinded spine with osteoblastic and osteolytic lesions.



## 5 From Algorithm to Prototype

The next step is the integration of the algorithm in a Siemens Healthcare Prototype User Interface. The development of new prototypes happens by MeVisLab with the syngo.via Frontier Development Kit (FDK). In this case the standard MeVisLab development environment is extended with components of the syngo.via Frontier application framework. This includes the syngo.via like user interface (UI) elements and the development documentation [57]. This prototype can be uploaded to the Frontier server. The research data base is the seamless connection between the research platform and the clinical infrastructure. Clinical partners of the Siemens Healthcare GmbH can evaluate the developed prototypes. It is necessary to get feedback from the partners to change the prototype for a better experience. An important point for this platform is, that the generated prototypes mostly are labeled with "not for clinical use". This means that the prototypes are only for research task and not for the clinical routine. Figure 5.1 shows the complete infrastructure of the Frontier environment. In the next sections the user interface design in syngo.via standard look and the interaction options for the advanced bone visualization algorithm will be described.

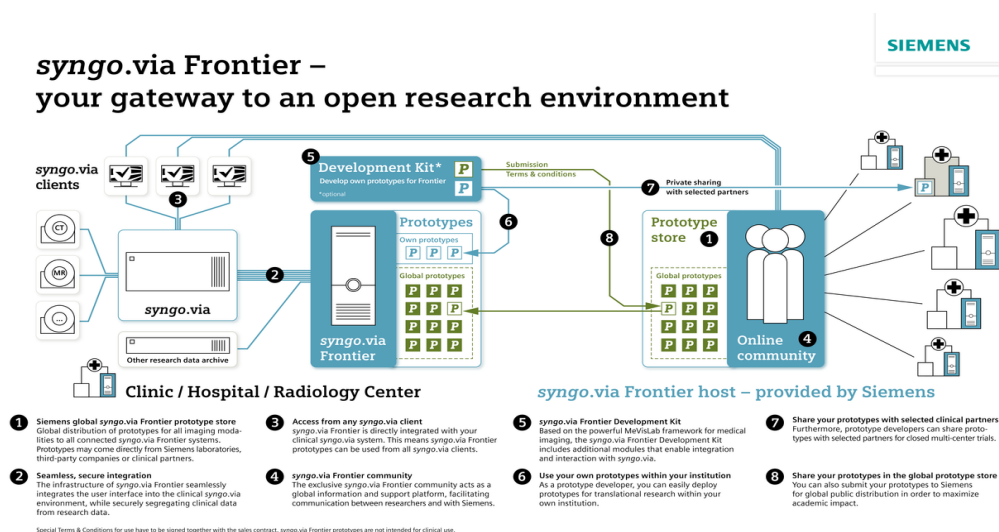


Figure 5.1: Syngo.via Frontier research environment overview.

## 5.1 User Interface Design

The complete design of the prototype is based on the syngo.via standard design rules [58]. This standard describes that the monitor screen includes two editable and one fixed areas. The first editable area is the monitor content area, which provides up to 20 viewers usable in predefined layouts. Furthermore, it has a snapshot functionality for each viewer segment and a blow-up functionality, which is provided for all viewer segments. The second editing area is the control area. This contains the layout switch button, common controls, algorithm controls, etc. The area can be customized with different buttons, MDL controls and more. The third not changeable area is the vortal area, which labeled the prototype as not for clinical use and connect the prototype with the data base. We present the three areas in the next step.

### Vortal Design

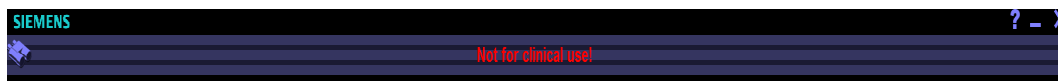


Figure 5.2: Vortal design of typical Siemens prototypes.

The vortal design is the not changeable instance of the prototype. (see Figure 5.2) On the upper left side is a binocular. This signalizes the connection from the UI to the patient browser. In this browser, the user can load a data set from a network data base, a local database, or the Picture Archiving and Communication System (PACS). Figure 5.3 shows the opened patient browser. Here the user can search for a data set by writing in the text area. With clicking on the binocular he accepts his input and the data base searches a possible data set. Another possibility to choose a data set is the "Tag search" on the right side of the patient browser. The patient browser lists all possible data set in the left table. Then the user can choose the data set and on the middle table each data of these data sets is shown. With the buttons on the lower side the user can see a preview of the data set or he can load the data set in the prototype. If the data set is loaded the MPR views are shown in the defined monitor content area. The label "Not for clinical use" shows the research status of the prototype.

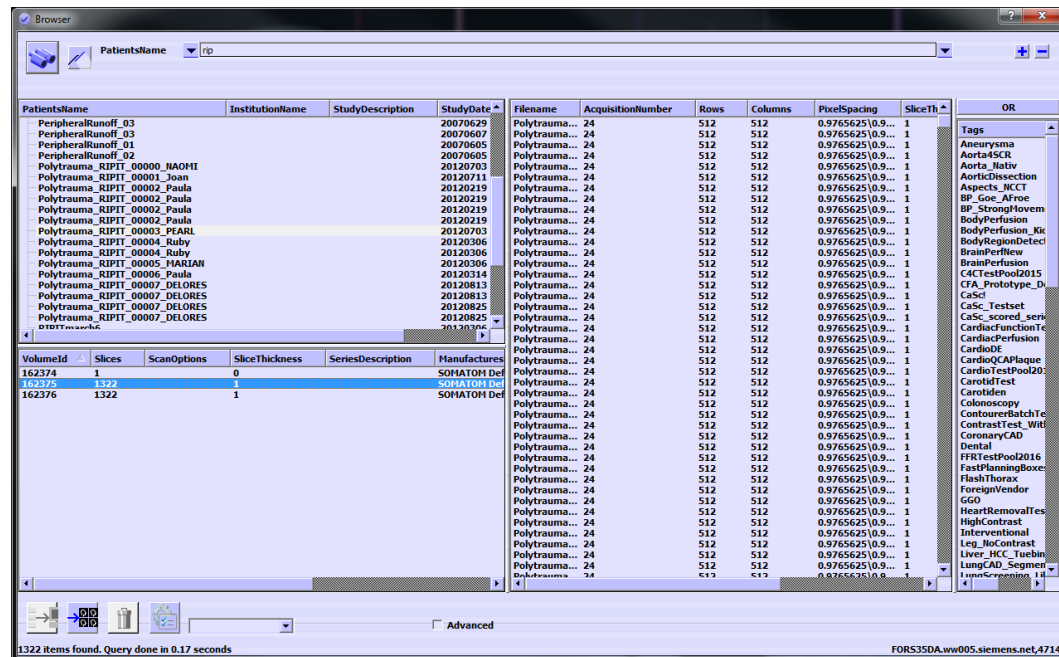


Figure 5.3: Patient browser interface to load a data set. The interface includes an tag search(Dicom-Tags, User-Defined-Tags, etc.) and an text edit search. The middle and left tables describe the data sets with the including data. The buttons on the bottom present a preview of the dataset or load this to the prototype.

### Monitor Content Area Design

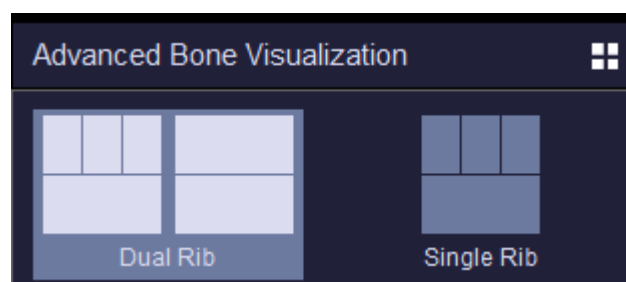


Figure 5.4: Possible defined layout options in the prototype.

The first task is the design of the screen layouts. Mostly the workstation of a radiologist has two monitors, but sometimes there is the possibility that they have only one screen. To create a prototype, which respects both necessities,

two different layouts must be designed for two screens and for one screen. The two screen variant includes on the first screen the standard MPR views and the unwinded image of the ribs. All interaction tasks are located on the first screen, in this case the layout change, the rib unfolding algorithm and the rib or spine unwinding options. On the second screen is on the upper half the result of the rib unfolded image shown and on the lower half the unwinded spine is located. The single screen layout is a reduced form of the two screen layout and includes the multi planar reformation views and the unwinded image, which is changeable to the spine or to the ribs. The layout selection is shown in Figure 5.4 and the different screen designs are shown in Figure 5.5 and Figure 5.6.

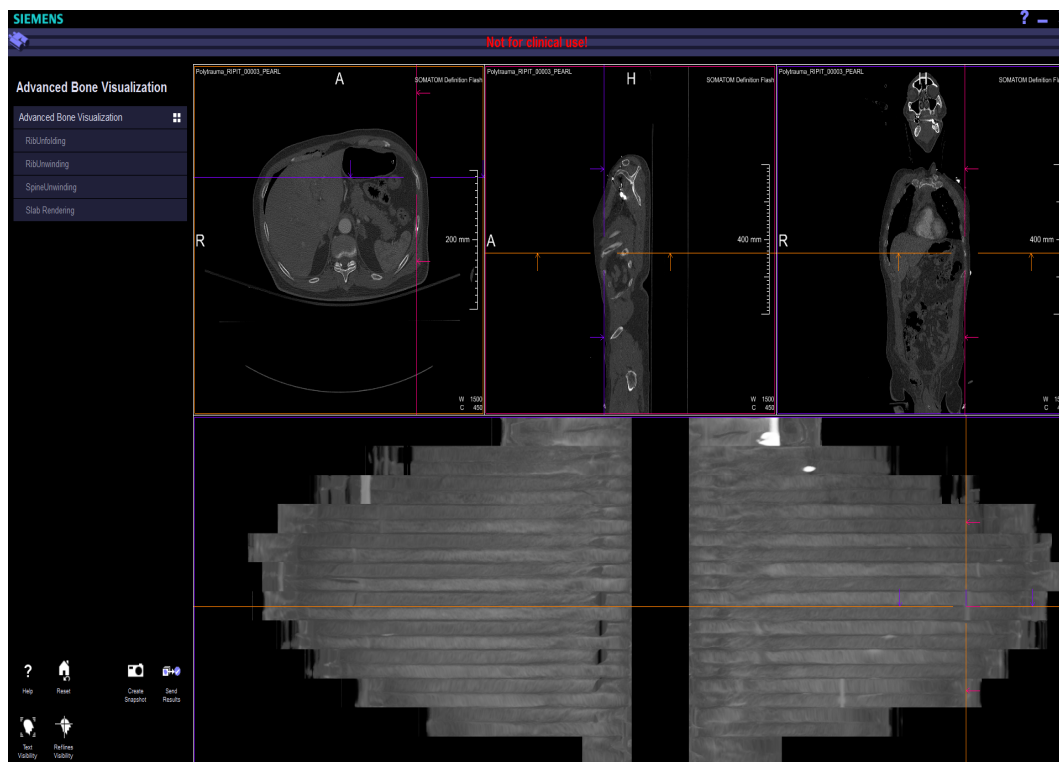


Figure 5.5: Single Screen alternative of the prototype.

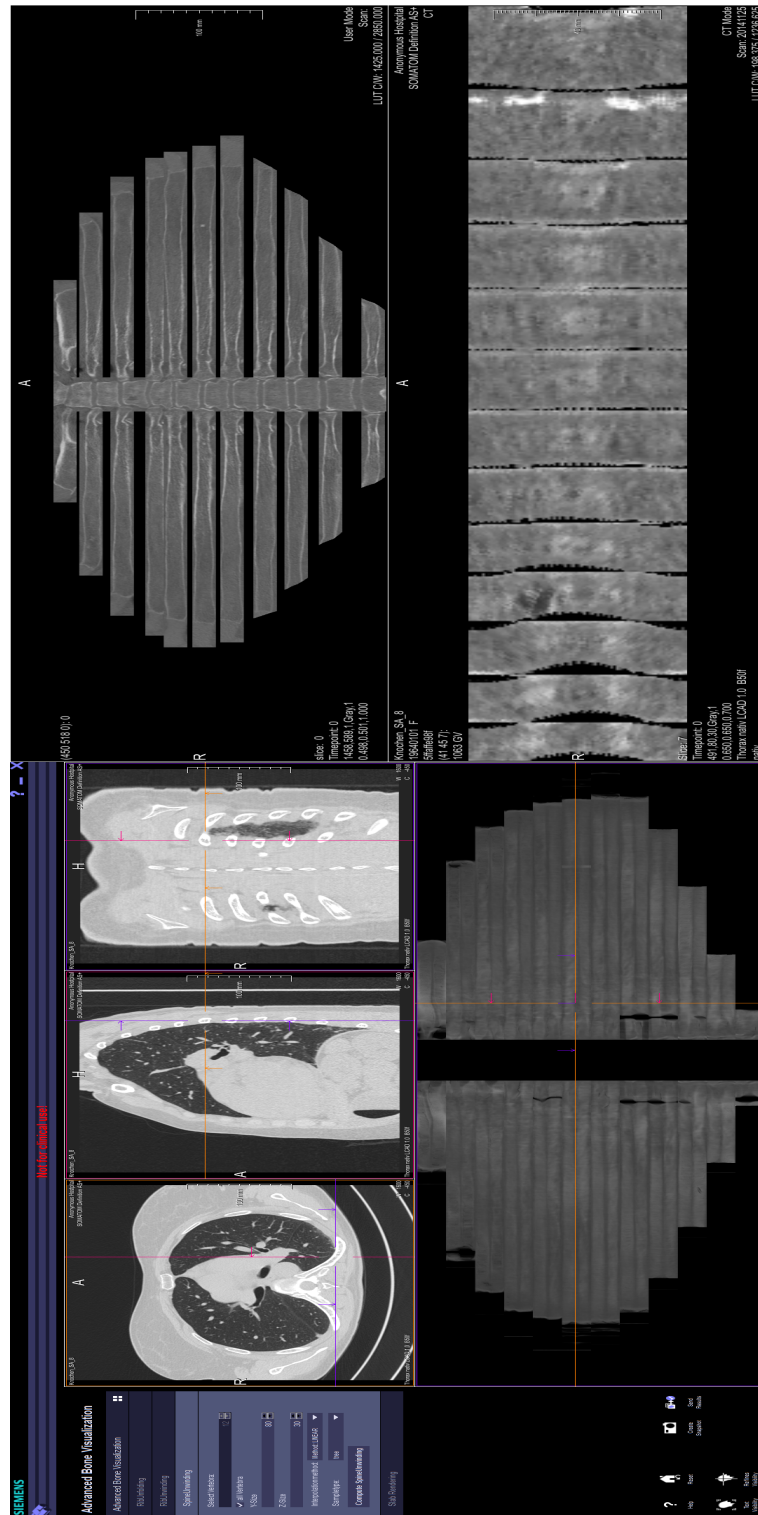
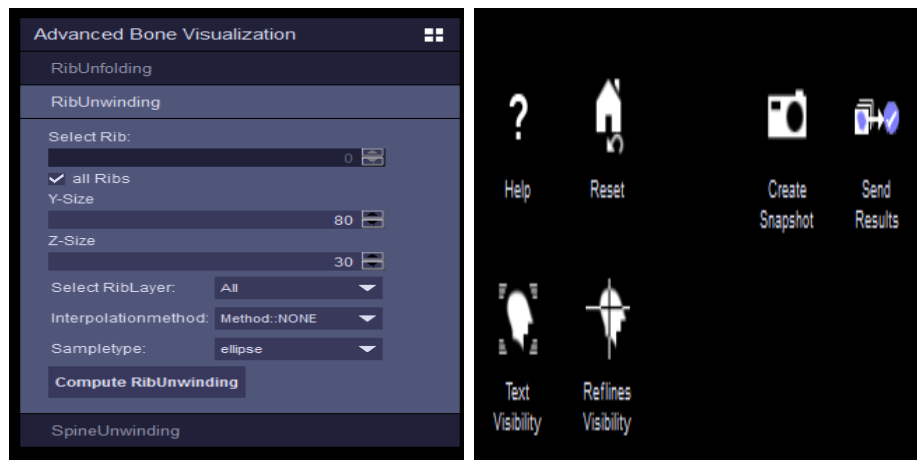


Figure 5.6: Complete two screen view of the Advanced Bone Visualization prototype.

## Control Area Design

The second changeable area is the control area, which processed required user inputs. According to the Syngo.via standard the area has four different components, which share on the left side of the first monitor. Each control area has exactly one main task. In this case it is the complete *Advanced Bone Visualization* algorithm. To realize the correct progress of the algorithm, the task is divided into different steps. Each step is a pop out menu, which will be opened by a click on it. The steps in the prototype are the precalculation of the rib unfolding, the rib unwinding or spine unwinding algorithm inputs and the slab rendering. The rib unfolding step includes a button to trigger the unfolding algorithm, which is requested for the unwinding algorithm. The next steps are the rib and the spine unwinding. Here the input values must be entered for the unwinding algorithm. For example the output image properties and the used sampling method. If the resulting image is calculated, the slab rendering follows. This pop out menu is for customizing the slab size and projection method. Apart from the task and step components there is the layout switch button, where the user can choose a suitable predefined monitor order. On the bottom of the control area are the common controls. Common controls are tools, which apply to the whole image area and which are not specific to the workflow. These tools are constant in the dedicated space and will not be changed. Examples for common tools include show/hide graphics, show/hide image text, send to film sheet, etc



(a) Popout menu Rib Unwinding step (b) Siemens Standard common tools

Figure 5.7: Advanced Bone Visualization prototype Control Area.

The different steps in the control area give the possibility to include interaction

options to the prototype. The user gets options to influence the algorithm or interact with the resulting image to support the pathology detection. The following section describes the included interaction methods and the percussions to the algorithm state and resulting images.

## 5.2 Interaction Options

### Selection of output image properties

The first interaction option is the output image property input. The user gives the wanted output image size, the sample angle steps and depth size number in the number edit. This influences directly the sample order in the algorithm. The next input data is the choose of the sampling method. The sampling method changes the used ray casting method in the algorithm. All input data must be accepted with the "Compute RibUnwinding" button. After trigger the button the algorithm starts and the direct feedback is the resulting unwinded image on the monitor content area. The input properties are the same for the rib unwinding and the spine unwinding. An example for the image property input is shown in Figure 5.8.

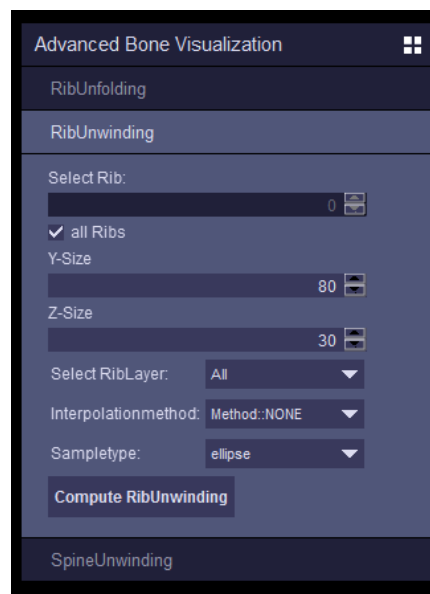


Figure 5.8: Example task for the rib unwinding algorithm. The user can choose the unwinding ribs, the resulting y- and z-size, the bone layer and the sample method.

### Adaption of the slab rendering

The included slab rendering needs an input by the user to adapt the different detection requirements. The slab size and projection method is changeable via a number edit for the slab size and a drop down menu for the projection method. This is given in the control area step "Slab Rendering". Here the slab size and projection method can be adapted (see Figure 5.9) and this has direct impact on the unwinded image.

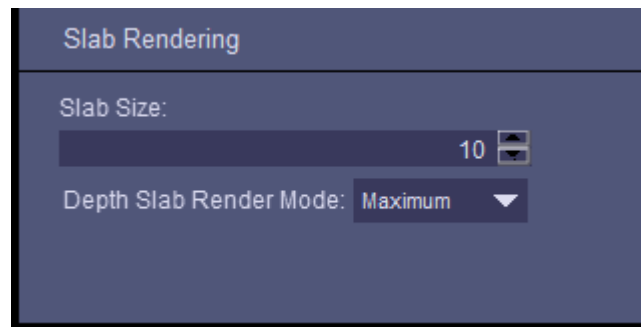


Figure 5.9: Design of the slab rendering step. The user can choose the slab size and the using projection method.

### Mouse Interaction

The mouse is the main input device for applications and is important for an analysis of a data set. The mouse is used for navigation within in the UI, selection and positioning. User interacts with objects on the UI by dragging the mouse and clicking on its buttons. The syngo.via standard use default primary and secondary mouse buttons, where the primary is the left mouse button and the secondary is the right button. The primary button in the prototype is primarily used to select and manipulate objects. For example, the user can zoom into an object to examine some structures in detail. Also, he can shift the reference line for the original recalculation. With the secondary mouse button the user can manipulate the image interactively by windowing and leveling. The third mouse button is the scroll wheel, which is used for scrolling, when the wheel is moved. During the interaction with the mouse some visual mouse pointers are added to provide visual feedback to the state of the interaction and its location within the screen area. The following table shows some of the mouse pointers, which are used in the prototype.












Shape	Name	Used when
	Normal Select	Used for most objects
	Select and move object	Used to indicate that an object can be moved with the mouse.
	Move line diagonally	Used on graphical objects to indicate that this object can be moved diagonally
	Move line horizontally	Used on graphical objects to indicate that this object can be moved horizontally
	Move line vertically	Used on graphical objects to indicate that this object can be moved vertically
	Rotate line	Used on graphical objects to indicate that this object can be rotated
	Resize diagonally	Used on graphical objects to indicate that this object can be resized diagonally
	Resize horizontally	Used on graphical objects to indicate that this object can be resized horizontally
	Resize vertically	Used on graphical objects to indicate that this object can be resized vertically

Table 5.1: Selection of mouse pointers for the prototype.

### Recalculation Original Position

As already announced in the *Advanced Bone Algorithm* chapter it is necessary to include a navigation from the unwinded image to the original data set. A good solution is a synchronize recalculation by reference lines. The reference lines describe the position in the unwinded visualization and there connected with the MPR views to get a correct view over the axial, sagittal and coronal view. The calculation is divided into two parts. At first the rib index must be identified to get the right centerline. The knowledge about the image size and the maximum rib number in combination with the position of the reference line, the rib index can be calculated. The left half of the unwinded image are the ribs over the half and on the right half are the first half of the ribs. Consequently the y-coordinate of the reference line is used to calculates the rib index. (Formula 5.2)

$$ribindex = \begin{cases} (y_{refpos}/inysize) + (ribnum/2), & \text{if } x_{refpos} < 1500 \\ y_{refpos}/inysize, & \text{if } x_{refpos} > 1700 \end{cases} \quad (5.1)$$

$$(5.2)$$

With the rib index and the corresponding centerline the correct position calculation follows. The x-position results from the x-position of the reference line and the point in the centerline point list. The y-position and z-position computation is based on the used ray casting method. Each method has another calculation rule, so different formula must be added to get the right position in the original space. The following formula shows the calculation for the adaptive and radial method. The main difference for the adaptive method is, that the ray length for the right angle must be dynamically detected by using ray casting. With the primary mouse button the user can move the reference line and the position will immediately update in the multi planar reformation views. Figure 5.10 visualizes this calculation on a partial fracture case.

$$\begin{bmatrix} x_{refpos} \\ y_{refpos} \\ z_{refpos} \end{bmatrix} \Rightarrow \begin{bmatrix} i \\ j \\ k \end{bmatrix} \quad (5.3)$$

$$\begin{bmatrix} x_{orig} \\ y_{orig} \\ z_{orig} \end{bmatrix} = S \cdot R(t_i, \varphi) \cdot n_i + p_i \quad (5.4)$$

where:

$$\varphi = \frac{j}{J} \cdot 2\pi \quad S = \frac{k}{K} \cdot d \quad (5.5)$$

with:

- $\begin{bmatrix} x_{refpos} \\ y_{refpos} \\ z_{refpos} \end{bmatrix}$ : is the reference line position
- $\begin{bmatrix} i \\ j \\ k \end{bmatrix}$ : is the mapped position of the reference line position
- $\begin{bmatrix} x_{orig} \\ y_{orig} \\ z_{orig} \end{bmatrix}$ : is the original position
- $R(t_i, \varphi) \cdot n_i$ : is the rotation from  $t_i$  around  $n_i$  about  $\varphi$
- $\frac{j}{J}$ : is the amonut from sampled  $y_{refpos}$  to  $y_{max}$
- $\frac{k}{K}$ : is the amonut from  $z_{refpos}$  to  $z_{max}$
- $d_i$ : raylength on point  $p_i$
- $p_i$ : is the point on the centerline
- $t_0$ : is the given upvector on  $p_i$
- $n_i$ : is the given tangential vector on  $p_i$

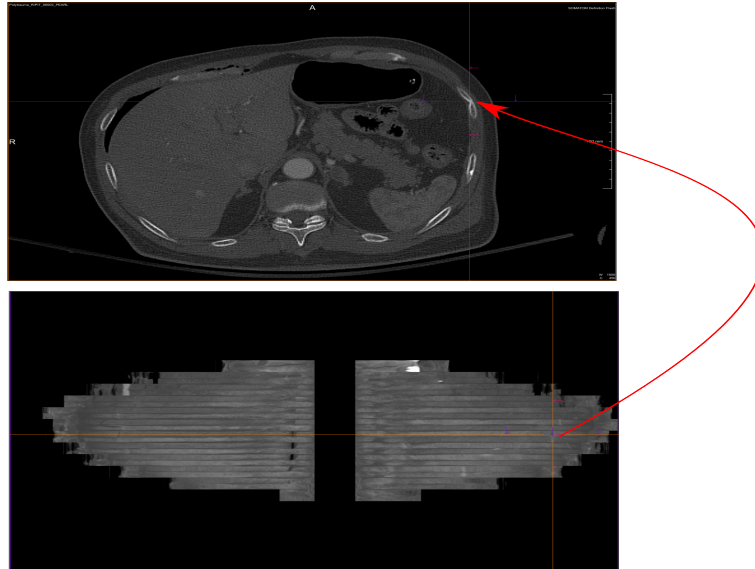


Figure 5.10: Illustration of synchronized navigation between unwinding image and axial MPR view to detect and verify a buckle fracture.

In this chapter the integration from the algorithm to a prototype was explained and which interaction methods are available to detect pathology. To analyze the quality of the algorithm and the prototype the next chapter includes a quantitative description of the algorithm accuracy and qualitative analysis of the complete prototype by clinical experts.

## 6 Evaluation

The following evaluation is divided in two parts. The first is the quantitative comparison, which will validate the algorithm. The quantitative comparison does not give an assessment about the clinical quality of the algorithm. Consequently, the second step is a qualitative evaluation with the complete prototype. The benefits of the new visualization technique to the rib unfolding will be tested and the handling of the developed prototype will be evaluated by experts.

### 6.1 Quantitative Comparison

#### 6.1.1 Test Cases

For the quantitative comparison 954 datasets with different scanning parameters were tested. The datasets were acquired with different CT scanners and reconstruction kernels. An independent test series is consequently warranted. The reconstruction kernel includes the principle of the reconstruction projection and the image characteristics, for example the resolution and noise. If a high contrast image is needed, the convolution kernel is high resolution and for a low contrast image a smoothing kernel is the necessary. This smoothing filter is used, because the low contrast structures will be overlapped by noise [9]. Furthermore the data sets include slice thicknesses between 0.5mm and 5mm. The slice thickness also affects influences to the noise of the images. A thin size gives a big resolution of the image, but with noise. To reduce it a bigger thickness can be used, but with the compromise that the resolution of the image and structures fall. Another influence of the slice thickness is the contrast resolution. These parameters are chosen for different usages. For example, a high resolution is required for small structures, like the inner ear. For the liver, a low spatial resolution is feasible. The liver need images with more contrast and further a bigger slice thickness can be chosen [24].

### 6.1.2 Results

In addition to the data sets all the three ray casting methods were tested. To save time the cubic interpolation was not used. Only the trilinear interpolation method was tested. In consideration of the given data sets 872 (91,4%) could be unwinded without failures. In 60 datasets (6,2%) missing ribs in the complete view occur. This can be due to missing centerlines from the rib unfolding algorithm or to segmentation failures. In 22 data sets (2,3%) the algorithm could not unwind the ribs, because the rib unfolding found no ribs and the unwinding algorithm did not start. After an analysis of the missing rib data sets the conclusion is, that the unwinding algorithm is a stable algorithm, if the rib unfolding algorithm before gives good centerlines and bounding boxes for the segmentation step. The average duration time of all tested data sets is one minute. The duration time is depending on the volume size and rib number of the given data set. Bigger volumes and more ribs rise the duration time.

## 6.2 Qualitive Comparison

At the time of the creation of the bachelor-thesis a big quality evaluation could not be realized, but there was the possibility to get suggestions by two clinical coaches, where one is specialized in trauma diagnoses and the other coach in oncological cases. Clinical coaches are the direct connection from the algorithm development to the clinical partners. They ensure the costumer views and necessities for the clinical workflow. A focus of their work is a appropriate execution from functionality and algorithm.

The following statements cannot replace an expert statement, however because of their user proximity their arguments are helpful.

### Test Conditions

The clinical coaches tested the prototype for an hour without contact to it before. The focus in the evaluation was the user experience in combination with the detection accuracy. Before they tested the Advanced Bone Visualization prototype they used the MPR and CT Bone Reading software to diagnose some data sets. The clinical coaches compared the results with the new visualization approach.

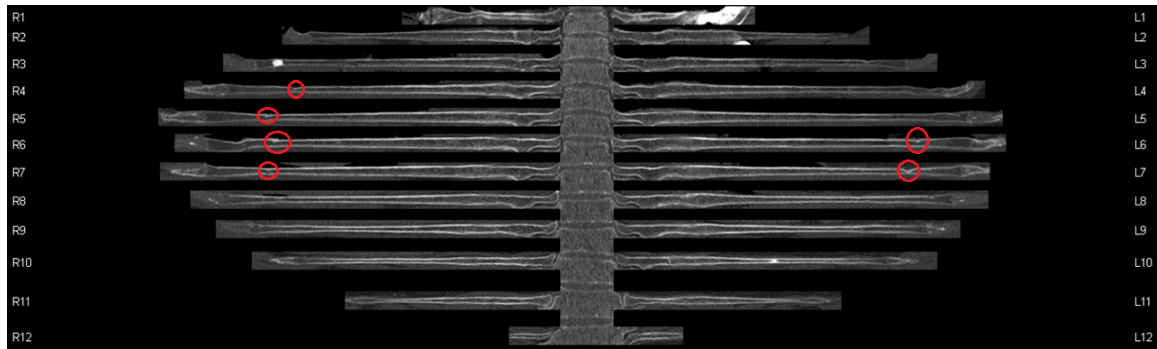


Figure 6.1: Example for an analyzed data with the CT Bone Reading.

### 6.2.1 Trauma Detection

For the trauma case three trauma data sets were analyzed and compared with the existing rib unfolding algorithm. The identification of complete fractures and displacements are easy to interpret. At this status of the prototype, the sometimes not perfect segmentation of the ribs, creates some dark holes in the unwinded image. These holes can wrong interpreted as buckled or partial fractures. Apart from this the identification of buckled and incomplete fracture is very intuitive and can be highlighted very good compared to the rib unfolding algorithm. Figure 6.2 shows some findings by the clinical coach in the unwinding image in connection with slab rendering an projection methods.

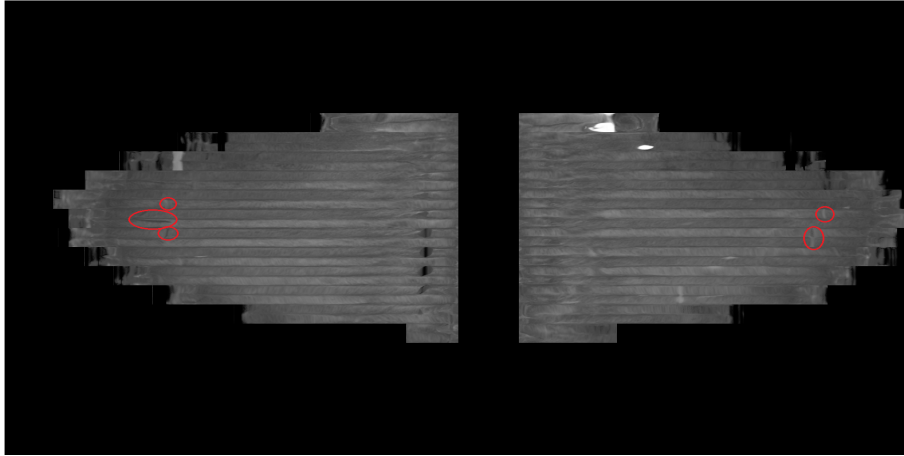


Figure 6.2: Findings of fractures in a rib unwinded image with maximum-intensity-projection. The circles are manually annotated pathologies by the clinical coaches.

### 6.2.2 Oncological Detection

In the detection of metastasis in the bone the clinical coach see a benefit in the visualization technique. The interaction in the rib unfolding is no need in this prototype and the overview of all ribs gives a good look on the ribs. The slab rendering in combination with a projection method highlight pathological areas very well and the synchronize between the MPR and the unwinded image helps in the orientation. Figure 6.3 shows an example of highlighted osteoblastic metastasis.



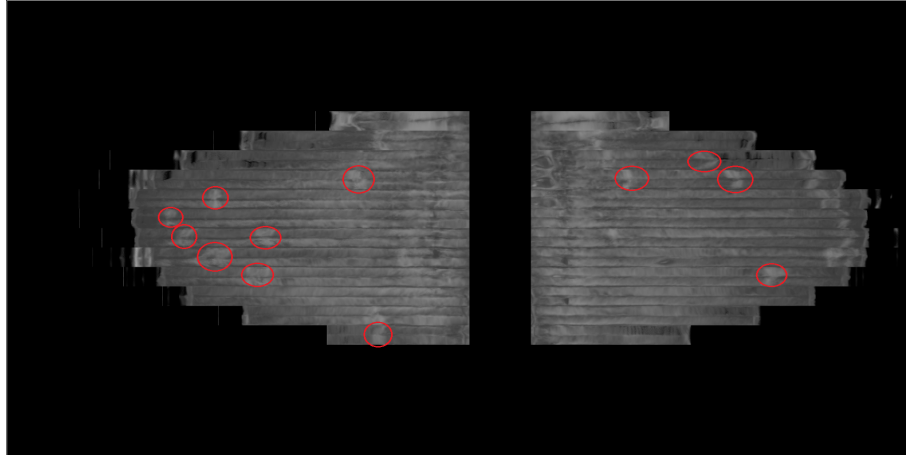


Figure 6.3: Good example for marked osteoblastic metastasis in the rib unwinded image. The circles are manually annotated pathologies by the clinical coaches.

### 6.2.3 Evaluation Conclusion

Both coaches explain that the program is a useful approach but must gain a better handling. In general the advanced visualization of the bones implicate many benefits against the existing rib unfolding algorithm and can realize a time saving in all cases. But the recalculation to the original data set is an important feature and necessary for a reliable detection of a pathology. Only the unwinded image without an context is difficult to interpret, which location is described.

Summarizing the prototype is a software with potential. The coaches see a benefit of this visualization method compared to the rib unfolding algorithm. Some failures in the segmentation state make the detection of pathologies harder. But they can imagine that a advanced version of the prototype is more accuracy than the CT Bone Reading. The lower interaction in the unwinding approach is very good to save time for choosing the correct therapy method.

## 7 Discussion

### 7.1 Conclusion

With this in the bachelor-thesis creating visualization method bones, in this case ribs and vertebrae, can be unwinded, that the entirety bone surface can be display in one view. Additional to the new visualization, underlying characteristics of the ribs in the unwinded image space can be mapped with a projection method (maximum-intensity-projection, minimum-intensity-projection, average). The interaction expense could be reduced to only interact with the slab rendering. The algorithm can be used with different elongated bone structures with an existing centerline. In the preprocessing step the bone can be divided and separated in predefined layers. Some over-segmented structures in the "inward" rib and vertebrae segmentation exist, but can be ignored for the following smoothing and unwinding steps. Terrace artifacts by the reconstruction from the raw data to the resulting image could be reduced by using a resampling approach. The integration of the algorithm in a frontier prototype enables user interaction and a qualitative evaluation by experts. The quantitative evaluation shows a stable and efficient algorithm with a big capability. Benefits for the unwinding algorithm in the different use cases exist in a qualitative evaluation by clinical coaches. Consequently, a technically sound algorithm was developed. This algorithm is a completely new visualization technique for bones, which can support the detection of bone pathology.

### 7.2 Future Work

The resulting prototype is a first version of a new visualization technique, so some implementation steps are not optimal. For example, the segmentation of the rib bone has the vertebra in it, which is not required for the unwinding algorithm and can be influence the resulting images. The smoothing method only reduce the present terrace artifacts, but they do not delete them completely and this can be very annoying in the image interpretation. A better smoothing or interpolation

method can be helpful to support the user experience. The unwinding image operates very well, but the resulting image composer step should separate each rib with a little spacing between each other. This supports the intuitive separation, which is in the current state of the prototype very difficult. Furthermore the spine and the ribs can be connected in one resulting image to have the complete rib cage in one overview, like in the Syngo.via CT Bone Reading. The slab rendering is a good approach to highlight pathology of the bones. An inclusion of the Siemens Healthcare Cinematic Renderer will extend the standard projection method with a illumination model to get a realistic view of the unwinded bones. The synchronized navigation by reference lines and the adaptability of the input are first interaction approaches. Maybe more methods, for example a measurement of distances or sizes of fractures and metastasis is a good and useful feature. Knowledge about size and course of a pathology can influence the following therapy methods. In this stage of the prototype algorithm a clinical usage is not possible. In addition the algorithm was tested for the spine and the ribs, some tests with other elongated bones must follow to support the hypothesis, that all elongated bone structures can be unwind. Maybe in a technically advanced stage the algorithm can be added to the CT-Bone Reading software in the Syngo.via. To realize this more tests and evaluation stages with clinical partners must follow.

# Bibliography

- [1] Paolo Angelelli and Helwig Hauser. Straightening tubular flow for side-by-side visualization. *IEEE transactions on visualization and computer graphics*, 17(12):2063–2070, 2011.
- [2] R. Bade. *Interaktive und dynamische Visualisierung fr die chirurgische Ausbildung und Interventionsplanung*. PhD thesis, Otto-von-Guericke University Magdeburg - Department of Simulation and Graphics, 2008.
- [3] Ragnar Bade, Jens Haase, and Bernhard Preim. Comparison of fundamental mesh smoothing algorithms for medical surface models. In *SimVis*, 2006.
- [4] Ragnar Bade, Olaf Konrad, and Bernhard Preim. Reducing Artifacts in Surface Meshes Extracted from Binary Volumes. *Journal of WSCG*, 15(1-3):67–74, 2007.
- [5] Bruce G. Baumgart. A polyhedron representation for computer vision. In *Proceedings of the May 19-22, 1975, National Computer Conference and Exposition*, AFIPS '75, pages 589–596, New York, NY, USA, 1975. ACM.
- [6] Georg Bier, Christoph Schabel, Ahmed Othman, Malte N. Bongers, Jrg Schmehl, Hendrik Ditt, Konstantin Nikolaou, Fabian Bamberg, and Mike Notohamiprodjo. Enhanced reading time efficiency by use of automatically unfolded CT rib reformations in acute trauma. *European Journal of Radiology*, 84(11):2173–2180, 2015.
- [7] G.J. Bryan. *Skeletal Anatomy*. Churchill Livingstone, 1996.
- [8] P. J. Burt. Fast filter transform for image processing\* 1. *Computer graphics and image processing*, 1981.
- [9] T.M. Buzug. *Einführung in die Computertomographie: Mathematisch-physikalische Grundlagen der Bildrekonstruktion*. Springer Berlin Heidelberg, 2005.
- [10] Enrico Contini. *Rib Cage Segmentation in CT Scans*. PhD thesis, Utrecht University - Faculty of Medicine Theses, 2013.

- [11] Philip Gabriel. *Experimentelle Studie zum Vergleich der Bildqualität von axialen Schnittbildern und multiplanaren Reformationen der Computertomographie anhand von Wirbelkörperpräparaten*. PhD thesis, Albert-Ludwigs-University Freiburg - Abteilung Röntgendiagnostik, 2004.
- [12] Catherine M Gdyczynski, Amir Manbachi, SayedMasoud Hashemi, Bahman Lashkari, and Richard S C Cobbold. On estimating the directionality distribution in pedicle trabecular bone from micro-ct images. *Physiological Measurement*, 35(12):2415, 2014.
- [13] LL Geyer, UJ Schoepf, FG Meinel, JW Nance, G Bastarrika, JA Leipsic, NS Paul, M Rengo, A Laghi, and CN De Cecco. State of the art: Iterative CT reconstruction techniques. *Radiology*, 276(5):339–57, 2015-08-01 00:00:00.001.
- [14] Maria Silvia Spinelli Giulio Maccauro. *Physiopathology of spinemetastasis*. 2011.
- [15] Andrew S. Glassner. Front matter. In *Graphics Gems*, pages iii –. Morgan Kaufmann, San Diego, 1990.
- [16] Rafael C. Gonzalez and Richard E. Woods. *Digital Image Processing (3rd Edition)*. Prentice-Hall, Inc., Upper Saddle River, NJ, USA, 2006.
- [17] T. A. Guise, K. S. Mohammad, G. Clines, E. G. Stebbins, D. H. Wong, L. S. Higgins, R. Vessella, E. Corey, S. Padalecki, L. Suva, and J. M. Chirgwin. Basic mechanisms responsible for osteolytic and osteoblastic bone metastases. *Clinical Cancer Research*, 12(20):6213s–6216s, 2006.
- [18] Frank Heckel, Michael Schwier, and Heinz-Otto Peitgen. Object-oriented application development with mevislab and python. In Stefan Fischer, Erik Maehle, and Rdiger Reischuk, editors, *GI Jahrestagung*, volume 154 of *LNI*, pages 1338–1351. GI, 2009.
- [19] Gabor T. Herman. *Fundamentals of Computerized Tomography: Image Reconstruction from Projections*. Springer Publishing Company, Incorporated, 2nd edition, 2009.
- [20] Georg Homann, Deedar F. Mustafa, Hendrik Ditt, Werner Spengler, Hans-Georg Kopp, Konstantin Nikolaou, and Marius Horger. Improved detection of bone metastases from lung cancer in the thoracic cage using 5- and 1-mm axial images versus a new CT software generating rib unfolding images. *Academic Radiology*, 22(4):505–512, 2015.
- [21] Jian Huang, Roni Yagel, Vassily Filippov, and Yair Kurzion. An accurate method for voxelizing polygon meshes. In *Proc. of the 1998 IEEE Symposium on Volume Visualization*, pages 119–126, 1998.

- [22] T. Huang, G. Yang, and G. Tang. A fast two-dimensional median filtering algorithm. *IEEE Transactions on Acoustics, Speech, and Signal Processing*, 27(1):13–18, 1979.
- [23] W.A. Kalender. *Computertomographie: Grundlagen, Gerätetechnologie, Bildqualität, Anwendungen*. Publicis-MCD-Verlag, 2000.
- [24] Willi A. Kalender. *Computertomographie-Grundlagen, Gerätetechnologie, Bildqualität, Anwendungen*. Publicis, 2. berarb. u. erw. auflage edition, 2006.
- [25] Rudolph Emil Kalman. A new approach to linear filtering and prediction problems. *Transactions of the ASME–Journal of Basic Engineering*, 82(Series D):35–45, 1960.
- [26] R. Keys. Cubic convolution interpolation for digital image processing. *Acoustics, Speech and Signal Processing, IEEE Transactions on*, 29(6):1153–1160, 1981.
- [27] Atilla P. Kiraly, Shuping Qing, and Hong Shen. A novel visualization method for the ribs within chest volume data, 2006.
- [28] Tobias Klinder, Cristian Lorenz, Jens von Berg, Sebastian P. M. Dries, Thomas Bülow, and Jörn Ostermann. *Automated Model-Based Rib Cage Segmentation and Labeling in CT Images*, pages 195–202. Springer Berlin Heidelberg, Berlin, Heidelberg, 2007.
- [29] Erwin Kreyszig. *Advanced Engineering Mathematics: Maple Computer Guide*. John Wiley & Sons, Inc., New York, NY, USA, 8th edition, 2000.
- [30] Jing Y. Krzeszinski and Yihong Wan. New therapeutic targets for cancer bone metastasis. *Trends in Pharmacological Sciences*, 36(6):360–373, 2015.
- [31] Jaesung Lee and Anthony P. Reeves. Segmentation of individual ribs from low-dose chest CT, 2010.
- [32] F. Lekien and J. Marsden. Tricubic interpolation in three dimensions. *International Journal for Numerical Methods in Engineering*, 63(3):455–471, 2005.
- [33] Benjamin D. Levine, Kambiz Motamedi, Kira Chow, Richard H. Gold, and Leanne L. Seeger. CT of rib lesions. *American Journal of Roentgenology*, 193(1):5–13, 2009.
- [34] William E. Lorensen and Harvey E. Cline. Marching cubes: A high resolution 3d surface construction algorithm. *SIGGRAPH Comput. Graph.*, 21(4):163–169, 1987.
- [35] Elaine Nicpon Marieb. *Human anatomy & physiology*. 2001.

- [36] Andre Marion. *Introduction to image processing*. Chapman and Hall, London, New York, Tokyo, 1991. Trad. de : Introduction aux techniques de traitement d'images.
- [37] MayfieldClinic. Anatomy of the spine, 2016.
- [38] Fraunhofer Mevis. [www.mevislab.de](http://www.mevislab.de), 2 2017.
- [39] T. Moench, S. Adler, and B. Preim. Staircase-aware smoothing of medical surface meshes. In *Proc. of Eurographics Conference on Visual Computing for Biology and Medicine*, pages 83–90, 2010.
- [40] S Napel, M P Marks, G D Rubin, M D Dake, C H McDonnell, S M Song, D R Enzmann, and R B Jeffrey. CT angiography with spiral CT and maximum intensity projection. *Radiology*, 185(2):607–610, 1992.
- [41] Sandy Napel, Geoffrey D. Rubin, and R. Brooke Jeffrey. STS-MIP: A new reconstruction technique for ct of the chest. *Journal of Computer Assisted Tomography*, 17(5):832–838, 1993.
- [42] H. Nyquist. Certain topics in telegraph transmission theory. *American Institute of Electrical Engineers, Transactions of the*, 47(2):617–644, 1928.
- [43] Francesca K. Ontell, Elizabeth H. Moore, Jo Anne O Shepard, and David K. Shelton. The costal cartilages in health and disease. *Radiographics*, 17(3):571–577, 1997.
- [44] Angelica Ortiz and Sue-Hwa Lin. *Osteolytic and Osteoblastic Bone Metastases: Two Extremes of the Same Spectrum?*, pages 225–233. Springer Berlin Heidelberg, Berlin, Heidelberg, 2012.
- [45] Merisa L. Piper, Lawrence Delrosario, and William Y. Hoffman. Distraction osteogenesis of multiple ribs for the treatment of acquired thoracic dystrophy. *Pediatrics*, 2016.
- [46] Bernhard Preim and Dirk Bartz. *Visualization in Medicine: Theory, Algorithms, and Applications*. Morgan Kaufmann Publishers Inc., San Francisco, CA, USA, 2007.
- [47] Bernhard Preim and Charl Botha. *Chapter 7 - Direct Volume Visualization*. Morgan Kaufmann, Boston, second edition edition, 2014.
- [48] Bernhard Preim and Charl Botha. *Chapter e14 - Projections and Reformations*. Morgan Kaufmann, Boston, second edition edition, 2014.

- [49] Harikrishna G. N. Rai and T. R. Gopalakrishnan Nair. Gradient based seeded region grow method for ct angiographic image segmentation. *CoRR*, abs/1001.3735, 2010.
- [50] Sowmya Ramakrishnan, Christopher Alvino, Leo Grady, and Atilla Kiraly. Automatic three-dimensional rib centerline extraction from ct scans for enhanced visualization and anatomical context. *Proc. SPIE*, 7962:79622X–79622X–12, 2011.
- [51] Helmut Ringl, Mathias Lazar, Michael Tpkker, Ramona Woitek, Helmut Prosch, Ulrika Asenbaum, Csilla Balassy, Daniel Toth, Michael Weber, Stefan Hajdu, Grzegorz Soza, Andreas Wimmer, and Thomas Mang. The ribs unfolded - a CT visualization algorithm for fast detection of rib fractures: effect on sensitivity and specificity in trauma patients. *European Radiology*, 25(7):1865–1874, 2015.
- [52] Scott D. Roth. Ray Casting for Modeling Solids. 18(2):109–144, 1982.
- [53] D. J. Sartoris, D. Resnick, D. Bielecki, D. Gershuni, and M. Meyers. Computed tomography with multiplanar reformation and three-dimensional image reconstruction in the preoperative evaluation of adult hip disease. *International Orthopaedics*, 12(1):1–8, 1988.
- [54] Claudia Schulze, Hanno Hoppe, Wolf Schweitzer, Nicole Schwendener, Silke Grabherr, and Christian Jackowski. Rib fractures at postmortem computed tomography (PMCT) validated against the autopsy. *Forensic Science International*, 233(1-3):90–98, 2013.
- [55] Jean Serra. *Image Analysis and Mathematical Morphology*. Academic Press, Inc., Orlando, FL, USA, 1983.
- [56] Jie Shuai. Novel multidimensional medical imaging using open source software. *SPIE Newsroom*, 2008.
- [57] Healthcare Siemens. *syngo.via Frontier - Your open platform for transational research*. 2016.
- [58] Healthcare Siemens. *User Interface Style Guide (Only for internal Use)*. 2016.
- [59] Gabriel Taubin. A signal processing approach to fair surface design. In *Proc. of ACM Conference on Computer Graphics and Interactive Techniques*, SIGGRAPH '95, pages 351–358, 1995.



- [60] Matthias Traub, Mark Stevenson, Suzanne McEvoy, Greg Briggs, Sing Kai Lo, Steven Leibman, and Tony Joseph. The use of chest computed tomography versus chest x-ray in patients with major blunt trauma. *Injury*, 38(1):43 – 47, 2007.
- [61] Frank Vogelsang, Frank Weiler, Joerg Dahmen, Markus W. Kilbinger, Berthold B. Wein, and Rolf W. Guenther. Detection and compensation of rib structures in chest radiographs for diagnostic assistance, 1998.
- [62] J. Vollmer, R. Mencl, and H. Mller. Improved laplacian smoothing of noisy surface meshes. *Computer Graphics Forum*, 18(3):131–138, 1999.
- [63] Jerold W. Wallis and Tom R. Miller. Volume rendering in three-dimensional display of spect images. *Journal of Nuclear Medicine*, 31(8):1421–1428, 1990.
- [64] Watt Mark Watt Allan. *Advanced Animation and Rendering Techniques: Theory and Practice*. ACM Press, 1992.
- [65] George Wolberg. *Digital Image Warping*. IEEE Computer Society Press, Los Alamitos, CA, USA, 1st edition, 1994.
- [66] Dijia Wu, David Liu, Zoltan Puskas, Chao Lu, Andreas Wimmer, Christian Tietjen, Grzegorz Soza, and Shaohua Kevin Zhou. A learning based deformable template matching method for automatic rib centerline extraction and labeling in CT images. In *2012 IEEE Conference on Computer Vision and Pattern Recognition, Providence, RI, USA, June 16-21, 2012*, pages 980–987, 2012.
- [67] [www.cancer.gov](http://www.cancer.gov). [www.cancer.gov](http://www.cancer.gov), 2017.
- [68] H. Zarqane, P. Viala, B. Dallaudière, H. Vernhet, C. Cyteval, and A. Larbi. Tumors of the rib. *Diagnostic and Interventional Imaging*, 94(11):1095–1108, 2013.